REPORT DOCUMENTATION PAGE	Form Approved OMB No. 0704-0188

1. AGENCY USE ONLY *(Leave blank)*	2. REPORT DATE	3. REPORT TYPE AND DATES COVERED
	21.Jun.00	THESIS

4. TITLE AND SUBTITLE
HURRICANE INNER-CORE STRUCTURE AS REVEALED BY GPS DROPWINDSONDES

5. FUNDING NUMBERS

6. AUTHOR(S)
CAPT LEEJOICE ROBERT N

7. PERFORMING ORGANIZATION NAME(S) AND ADDRESS(ES)
COLORADO STATE UNIVERSITY

8. PERFORMING ORGANIZATION REPORT NUMBER

9. SPONSORING/MONITORING AGENCY NAME(S) AND ADDRESS(ES)
THE DEPARTMENT OF THE AIR FORCE
AFIT/CIA, BLDG 125
2950 P STREET
WPAFB OH 45433

10. SPONSORING/MONITORING AGENCY REPORT NUMBER
FY00-222

11. SUPPLEMENTARY NOTES

12a. DISTRIBUTION AVAILABILITY STATEMENT
Unlimited distribution
In Accordance With AFI 35-205/AFIT Sup 1

12b. DISTRIBUTION CODE

13. ABSTRACT *(Maximum 200 words)*

14. SUBJECT TERMS			15. NUMBER OF PAGES
			16. PRICE CODE
17. SECURITY CLASSIFICATION OF REPORT	18. SECURITY CLASSIFICATION OF THIS PAGE	19. SECURITY CLASSIFICATION OF ABSTRACT	20. LIMITATION OF ABSTRACT

THESIS

HURRICANE INNER-CORE STRUCTURE AS REVEALED BY GPS DROPWINDSONDES

Submitted by

Robert N. LeeJoice

Department of Atmospheric Science

In partial fulfillment of the requirements

for the Degree of Master of Science

Colorado State University

Fort Collins, Colorado

Summer 2000

ABSTRACT OF THESIS

HURRICANE INNER-CORE STRUCTURE AS REVEALED BY GPS DROPWINDSONDES

New high-resolution information of the vertical thermodynamic and kinematic structure of the hurricane inner-core is now available from aircraft released Global Positioning System (GPS) dropwindsondes. This is a great technical advancement because now it is possible to sample the inner-core structure of tropical storms in detail. This study presents insights concerning the structure of mature hurricanes from dropwindsonde data obtained during the 1997 and 1998 hurricane seasons. Storm center fixes enable the inner-core calculation of radial and tangential winds. It will be shown that the radial inflow around the eye-wall cloud is approximately twice as large as that determined from frictional forcing. Air sea-surface temperature difference near the surface is in the 3-4°C range, not the 1°C differential previously assumed. Resulting θ_e values within the eyewall are found to be between 355-360K, which confirms with aircraft observations. The observed vertical gradient of θ_e in the eyewall region coupled with the inflow greater than expected from frictional forcing, implies an additional physical mechanism for such inflow. It is hypothesized that this additional mechanism is wall cloud buoyancy. Additionally, it is shown that the frictionally driven boundary layer is 1Km deep. This is determined by the depth of the inflow layer of the radial wind. The vertical gradient of the radial wind within the boundary layer provides insight to the current strength of tropical storms. Further analysis of this dropwindsonde data will lead too improved understanding of the hurricane inner-core region.

Robert N. LeeJoice
Atmospheric Science Department
Colorado State University
Fort Collins, CO 80523
Summer 2000

ACKNOWLEDGEMENTS

I would like to thank the Hurricane Research Division for access to their data, without which this study would've been impossible. Special appreciation goes to Robert Burpee and James Franklin whose work over the last 20 years on the Omega and GPS dropwindsondes has pioneered a new understanding of hurricane structure and an improvement in track forecasts. I would also like to thank my advisor William M. Gray for his extremely open door policy and his enthusiasm to help provide insight, guidance, and support during my time working for him. I wish to thank my committee members Professors Thomas Vonderhaar and Bob Meroney for helping me complete this work.

Special appreciation goes several people who helped me over the last couple of years in my quest to finish my degree. First, I must thank Freddi Boston who helped me find the multitude of papers within the atmospheric sciences library that I needed for this work. Second, Matt Eastin for providing the perspective of someone that has walked my path before and helping correct my course on numerous occasions. Third, Brian McNoldy for discussions and assistance with programming techniques that I used to analyze my data.

I would also like to thank the members of the Gray project for their help and assistance in preparing this thesis, the members of the Colorado State Field Hockey team for all the great memories, and the fellowship provided from the other Air Force officers here in pursuit of advanced degrees.

I must also thank my parents for all the support over the years that enabled me to reach this point and to the United States Air Force that gave me this great opportunity to achieve my master's degree.

Lastly, I must thank Jennifer Stewart for all her support, encouragement, patience, and caring over the last year. May our paths continue together.

TABLE OF CONTENTS

1 INTRODUCTION 1
1.1 Research Motivation 1
1.2 Objectives 2

2 OVERVIEW OF DROPWINDSONDES 4
2.1 Dropwindsonde History 4
2.2 The NCAR GPS Dropwindsonde 9
2.2.1 NCAR GPS Dropwindsonde Performance Specifications 9
2.3 Dropwindsonde Accuracy Improvements 12

3 DATA 14
3.1 GPS Dropwindsonde Data 14
3.2 Best-Track Data 17
3.3 Two-Minute Data 18

4 RADIAL AND TANGENTIAL WIND ANALYSIS 25
4.1 Radial and Tangential Wind Derivation 25
4.2 Radial Wind Determination from Friction 26
4.3 Comparison of Observed Radial Winds to Frictionally Induced Radial Winds 27
4.4 Role of the Vertical Gradient of the Radial Wind in Determining Storm Intensity 30
4.5 Conclusion 36

5. HURRICANE THERMODYNAMICS 37
5.1 Temperature and Potential Temperature Profiles 37
5.2 Relative Humidity and Specific Humidity Profiles 39
5.3 Equivalent Potential Temperature Profiles 40
5.4 Eyewall Surface Thermodynamic Parameters 42
5.5 Summary and Discussion 46

6. CONCLUSIONS 47
6.1 Summary and Discussion 47
6.2 Future Work 47

REFERENCES 49

A DROPWINDSONDE DATA FILES 52
A.1 Data Amount 52
A.2 Data File Types 52

LIST OF SYMBOLS AND ACRONYMS

AOC:	Aircraft Operations Center
AOML:	Atlantic Oceanographic and Meteorological Laboratory
AMS	American Meteorology Society
AVAPS:	Airborne Vertical Atmospheric Profiling System
AXBTs:	Airborne Expendable Bathothermal graphs
°C:	Degree Celsius
CIRA:	Cooperative Institute for Research of the Atmosphere
DDT:	Digital Dvorak Technique
ERICA:	Experiment on Rapid Intensification of Cyclones over the Atlantic
GARP:	Global Atmospheric Research Program
GATE:	Global Atmospheric Research Program Atlantic Tropical Experiment
GFDL:	Geophysical Fluid Dynamics Laboratory
GPS:	Global Positioning System
h:	Hour
HRD:	Hurricane Research Division
K:	Kelvin
km:	Kilometer
L2D2:	Lightweight Loran Digital Dropwindsonde
mb:	Millibar
MSLP:	Minimum Sea Level Pressure
NCAR:	National Center for Atmospheric Research
nm:	Nautical miles
NOAA:	National Oceanographic and Atmospheric Administration
ODT:	Objective Dvorak Technique
ODW:	Omega Dropwindsonde
ONS:	Omega Navigation System
θ	Potential Temperature
q:	Specific Humidity
RH:	Relative Humidity
s:	Second
t:	Temperature
θ_e:	Equivalent potential temperature or theta-e
Vr:	Radial Wind Speed
Vt:	Tangential Wind Speed

Chapter 1

INTRODUCTION

1.1 Research Motivation

Tropical storm forecasters have only satellite-based techniques to monitor tropical storms in the majority of the world. Geostationary satellites with infrared (IR) and visible (VIS) sensors have been the mainstay of tropical storm forecasting since their launch in the mid 1960s. Indeed, Vernon Dvorak, in 1975, published a method for forecasting tropical storms from solely VIS imagery. In 1984, he extended his method through the use of IR as well as VIS imagery. Even more reliance on satellite based forecasting of tropical storms occurred in 1987 when the United States Air Force (USAF) ceased operational reconnaissance flights into tropical storms from Guam.

Today the United States is the only country that performs tropical storm reconnaissance flights for both operational and research objectives. The flights are primarily undertaken in the western Atlantic, Caribbean, and Gulf of Mexico regions by the Hurricane Research Division (HRD) and the Air Operations Center (AOC) of the National Oceanographic and Atmospheric Administration (NOAA). On these missions Global Position System (GPS) dropwindsondes are released into the core and the outer regions of the storms.

The recently developed dropwindsonde technology provides unprecedented vertical resolution and accuracy of kinematic and thermodynamic properties within the hurricane's inner core. Figure 1.1 shows the strongest dropwindsonde measured wind speed from the 1997 and 1998 seasons at 93.6 m/s from one dropwindsonde dropped into hurricane Mitch on Oct 27, 1998. This value exceeds the previous dropwindsonde measured peak wind of 91 ms^{-1} found within hurricane Georges (Franklin, et al., 1999).

It is important to take advantage of this data and apply it to improve our understanding of hurricane structure and dynamics. It is also vital to publish this new knowledge so that other areas of

the world, that don't have access to this data, can supplement their satellite forecasting techniques.

1.2 Objectives

GPS dropwindsondes released during tropical storm reconnaissance flights provide unprecedented vertical resolution into the wind structure and thermodynamics of tropical storms. This high-resolution data will help explore two research objectives. First, inner core radial and tangential winds will be analyzed to study inner-core dynamic characteristics of hurricanes. Second, a preliminary look at the thermodynamic parameters from surface and vertical profile perspectives will be presented to further our understanding of hurricane thermodynamics.

Chapter 2 will present a short history of the use of dropwindsonde data as well as the accuracy of the data. Chapter 3 contains a discussion of what datasets were used, how they were obtained, and what for they were used. Chapter 4 deals with radial and tangential wind profiles taken from 6 different hurricanes during the 1997 and 1998 seasons. Chapter 5 presents the thermodynamic parameters, while conclusions and perspective for future work are presented in chapter 6.

Note: dropwindsonde, dropsonde, and sonde will be used interchangeably throughout this thesis. However, the term dropsonde will be emphasized, because these instruments measure both thermodynamics and wind speeds, not just the latter.

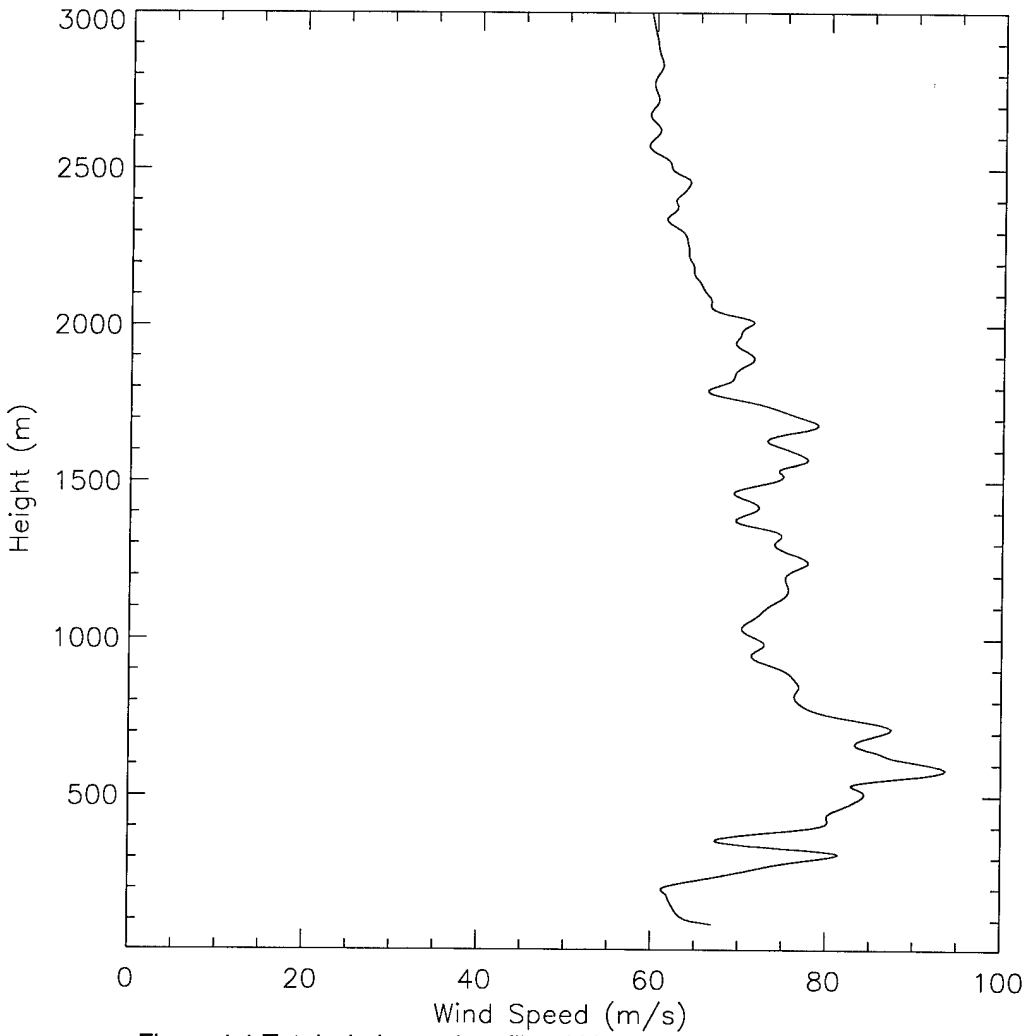

Figure 1.1 Total wind speed profile within the eyewall of Hurricane Mitch at 2243 UTC 27 October 1998.

Chapter 2

OVERVIEW OF DROPWINDSONDES

2.1 Dropwindsonde History

John Beukers, in the early 1960's, first proposed that upper air measurements of wind speed and thermodynamic parameters could be taken by sondes dropped from aircraft (Scribner and Smalley 1981). Beukers Laboratories, owned by John Beukers, developed a dropsonde and tracking system that worked in 1967. The equipment was used in the Global Atmospheric Research Program's (GARP) Atlantic Tropical Experiment (GATE) in 1972. The GATE experiment was the first experiment that obtained upper air data from aircraft altitude to near ocean surface (Simpson et al., 1975). More importantly it was the first time that upper air data could be obtained over oceans without the use of ships launching rawindsondes. Aircraft with their range and mobility ushered in a new era of research over the tropics.

The National Center for Atmospheric Research (NCAR) entered into the scene in the mid 1970's, when they entered into agreement with GARP to improve the sonde used in GATE. NCAR continued to improve the design and the instrumentation of the sonde over the next several years. NCAR's effort cumulated when design specifications were finalized and a contract for production of 7,500 sondes was awarded in 1977.

These sondes became known as Omega dropwindsondes (ODWs) because of their use of Omega navigational signals. The Omega Navigation System (ONS) was a system developed from work in the 1940's to provide worldwide navigation to within 2 nautical mile accuracy. It was an international effort with 8 stations that provided global coverage (Richardson 1974). By using the Omega navigation signals, these dropwindsondes could be deployed in any research experiment in the world. In fact, GARP successively used over 5000 Omega dropwindsondes during the special observing periods of the GARP sponsored Global Weather Experiment (Julian, 1982).

An important extension to the use of the Omega dropwindsondes occurred in 1982 when the Hurricane Research Division (HRD) deployed them around hurricane Debby. Using the results from the experiment, Burpee et al. (1984) suggested that hurricane forecast tracks could be improved by releasing dropwindsondes around tropical storms and incorporating their data into numerical models. Burpee argued that since satellites infer winds by cloud motions in the layer between 9 and 12 km and low-level observations measure the lowest 2 km, a critical layer of data was missing. This insight was a follow-on to Neumann's (1981) argument that a major reason for the slower rate of improvement of track forecasts were due to a decline in observing platforms in the subtropics from the 1960's and 1970's. Burpee's hypothesis was based on the observation that the best steering level of the tropical cyclone is at mid tropospheric levels (George and Gray 1976). In his view, the deployment of ODWs would provide the needed data to improve track forecasts.

One significant result of Burpee's work was the determination of an ideal flight reconnaissance pattern (Figure 2.1). In this ideal pattern, flight legs were separated by 3° latitude and ODWs were released at intervals 1.5° along the track. This pattern was based on the view that gradients of the wind field and thermodynamic variables perpendicular to the storm track helped determine storm motion. Therefore, tropical cyclone flight patterns were oriented with respect to the storm heading so that cross-track gradients could be measured.

Burpee only had the Debby case to try to prove his point about improving track forecasts. Of course one case was not enough to draw any conclusions. However, what came out of that work was a commitment by the HRD to provide funding for several more missions during the 1980's to deploy dropwindsondes into tropical storms with the intention of developing a large enough database to study if the use of dropwindsonde helped improve track forecasts.

Flying around tropical storms and releasing dropsondes became known as synoptic surveillance flights (Franklin and DeMaria 1992). The AOC's two P-3 turboprop aircraft performed these synoptic surveillance missions collecting data within 1000 km of storm center. By the mid-1990s enough Omega dropsonde data was available (Table 2.1) to test Burpee's hypothesis that sondes released to measure the environment around tropical storms could improve track model

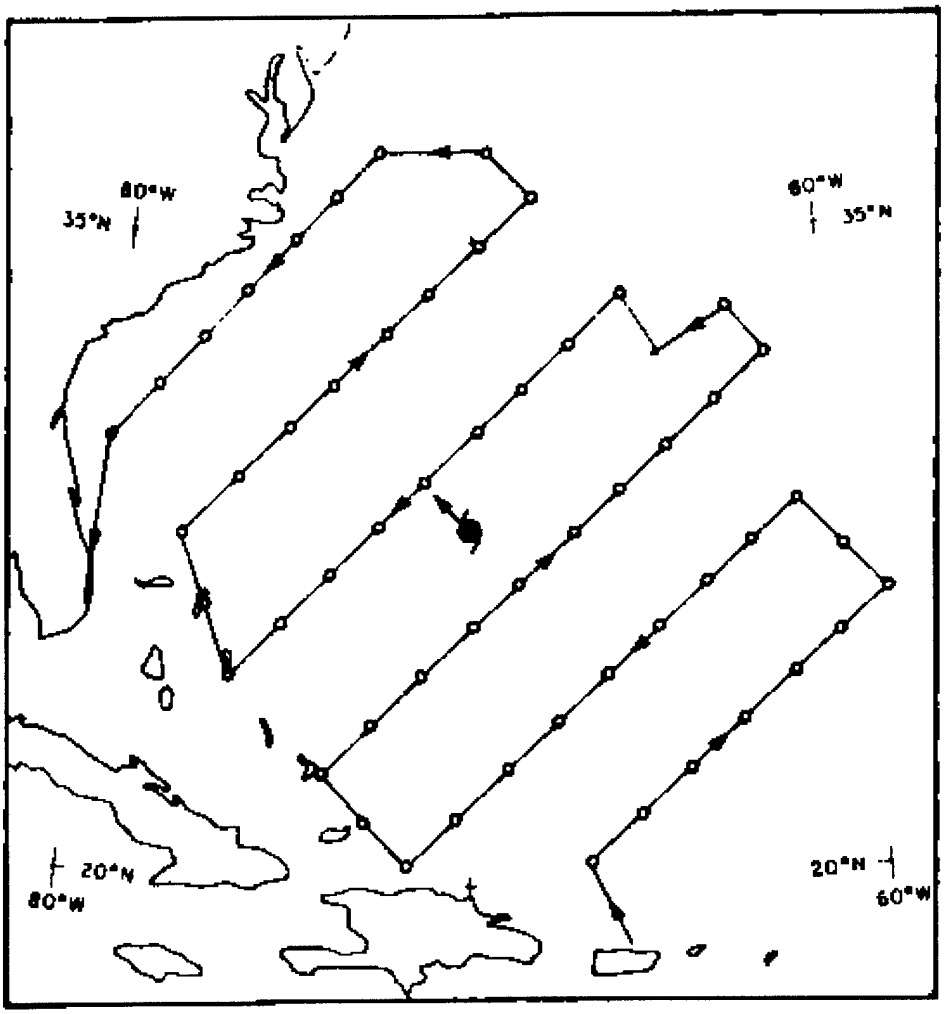

Figure 2.1: Idealized flight pattern for dropwindsonde experiment. One aircraft start in Bermuda and flies to Miami at the end of the mission. The second aircraft takes off from San Juan and completes its mission in Bermuda. The location of a hypothetical hurricane that is moving toward the northwest is at 28.° N, 70° W. The locations of ODWs are represented by the open circles. From Burpee, et al. 1984.

forecasts. Indeed, several people worked on this to include Burpee et al. (1996), Franklin and DeMaria (1992), Tuleya and Lord (1997), and Heming (1999).

Table 2.1: Synoptic flow experiments conducted in Atlantic tropical cyclones. The time is the standard observation time for the experiment, and the storm strength (SS) is indicated by an H for hurricane or TS for tropical storm. Also shown are the number of aircraft participating in an experiment and the number of successful ODWs. From Burpee et al. 1996.

	Storm Name	SS	Date/time at 0000 (UTC) unless noted	Number of aircraft/number of ODWs
1	Debby	H	15-Sep-82	1/29
2	Debby	H	16-Sep-82	2/49
3	Josephine	TS	10-Oct-84	1/24
4	Josephine	H	12-Oct-84	1/23
5	Josephine	H	12-Oct-84	1/23
6	Gloria	H	25-Sep-85	2/53
7	Emily	TS	24-Sep-87	1/30
8	Emily	TS	25-Sep-87	2/53
9	Floyd	TS	11-Oct-87	2/53
10	Floyd	TS	12-Oct-87	1/29
11	Florence	TS	9-Sep-88	2/51
12	Hugo	H	20-Sep-89	1/24
13	Hugo	H	21-Sep-89	1/29
14	Jerry	TS	14-Oct-89/1200	1/20
15	Bob	H	18-Aug-91	1/14
16	Andrew	H	23-Aug-92	2/49
17	Emily	H	30-Aug-93	1/22
18	Emily	H	31-Aug-93	1/19

Track forecast results depend on the model to which the dropwindsonde data are applied. For example, Franklin and DeMaria (1992) found that track forecast errors were reduced from 12-16% when dropwindsonde data was added to the VICBAR model (Aberson and DeMaria, 1994). Tuleya and Lord (1997) found that mean track errors were reduced by 12 km at 12 h, by approximately 50 km for 24-60 h, and by 127 km at 72 h when applied to the Geophysical Fluid Dynamics Laboratory (GFDL) high resolution regional forecast model. Bupree et al. (1996), returning to his hypothesis over a decade later, also found that dropwindsonde observations improved track forecasts by 16-30% when a consensus forecast from three numerical models was used.

While HRD was using the Omega dropsondes for hurricane research during the 1980s, NCAR started developing a new light-weight digital dropsonde to support the Office of Naval Research's Experiment on Rapid Intensification of Cyclones over the Atlantic (ERICA) in 1987 (Hock 1999). The dropsonde was known as the Lightweight Loran Digital Dropwindsonde or L2D2. The dropsonde was developed because the Omega dropsondes were not accurate enough for the research-quality winds needed for ERICA (Lally et al. 1989). Actually, in 1985 NCAR proposed that a GPS dropsonde be used for ERICA, but the Challenger disaster set the GPS satellite launch cycle back and Loran based navigation was the fallback plan. In essence, the L2D2 provided an improved dropsonde over Omega and an interim solution until the GPS dropsonde was developed.

As a result of some of the hurricane track improvement studies, work began in the early 1990's to procure an aircraft that could provide high altitude, high speed, long range, and the payload capability required for an operational and research airborne platform for the 21st century (White et al. 1998; Franklin et al., 1999). The aircraft acquired was a Gulfstream IV-SP (G-IV) jet. The new jet aircraft joins the AOC's two P-3 turboprop aircraft for hurricane research. The G-IV can operate up to 150 mb and has a range of 4000 nm. (The P-3s are more limited; having a ceiling of 350 mb and have a range of 2950 km.) The G-IV will perform the synoptic surveillance missions due to its ceiling and range attributes, while the P-3s will continue to fly into the inner core of tropical storms and hurricanes.

A multiple of factors came together requiring that a new dropsonde be developed. First, ODWs weren't designed to be deployed at jet aircraft speeds. Second the existing navigation networks were ceasing operation do to full operational status of the GPS network. In fact, by the early 1990s the demise of the Omega Navigation System was evident. There was no need for 2 nm accuracy when 30-meter accuracy could be obtained with GPS navigation. The Omega Navigation System was terminated on September 30, 1997 (United States Coast Guard, 1996) and the Loran navigation soon after. NCAR was once again at the drawing board developing the 21st century dropsonde.

2.2 The NCAR GPS Dropwindsonde

NCAR built upon its experience with the L2D2 to create the GPS dropwindsonde. For example, the parachute used by the L2D2 is the same used by the GPS dropsonde and many of the component parts are just improvements over those used in the L2D2. Figure 2.2 shows both assembled and internal views of the GPS dropwindsonde. The sonde's dimensions consist of a 7 cm diameter and a 41 cm length. Besides being small, the GPS dropsonde is quite light weighing only 400 grams. The sonde has 3 main components that will be described presently. The pressure, temperature, and humidity (PTH) senor provides highly accurate measurement of these parameters through a wide range of atmospheric conditions (Table 2.2). The GPS receiver records the relative Doppler frequencies from the GPS satellite signals, which represent the combined motion of the satellite and dropsonde. The GPS receiver works in conjunction with the 400 MHz transmitter to transmit the PTH data as well as the GPS telemetry data to the aircraft. The digital microprocessor unit controls the overall function of the dropwindsonde. .

Table 2.2: Estimated typical measurement errors for the NCAR GPS dropwindsonde. From Hock and Franklin (1999).

Parameter	Typical Error
Pressure	1.0mb
Temperature	0.2 C
Humidity	< 5%
Wind	0.5 - 2.0 m/s

2.2.1 NCAR GPS Dropwindsonde Performance Specifications

Multiple organizations provided design specifications for the NCAR GPS dropwindsonde. The principle agents involved were NCAR, NOAA, and the German Aerospace Research Establishment. Some of the combined requirements follow:

- Operations up to altitudes of 24 km
- Global operation

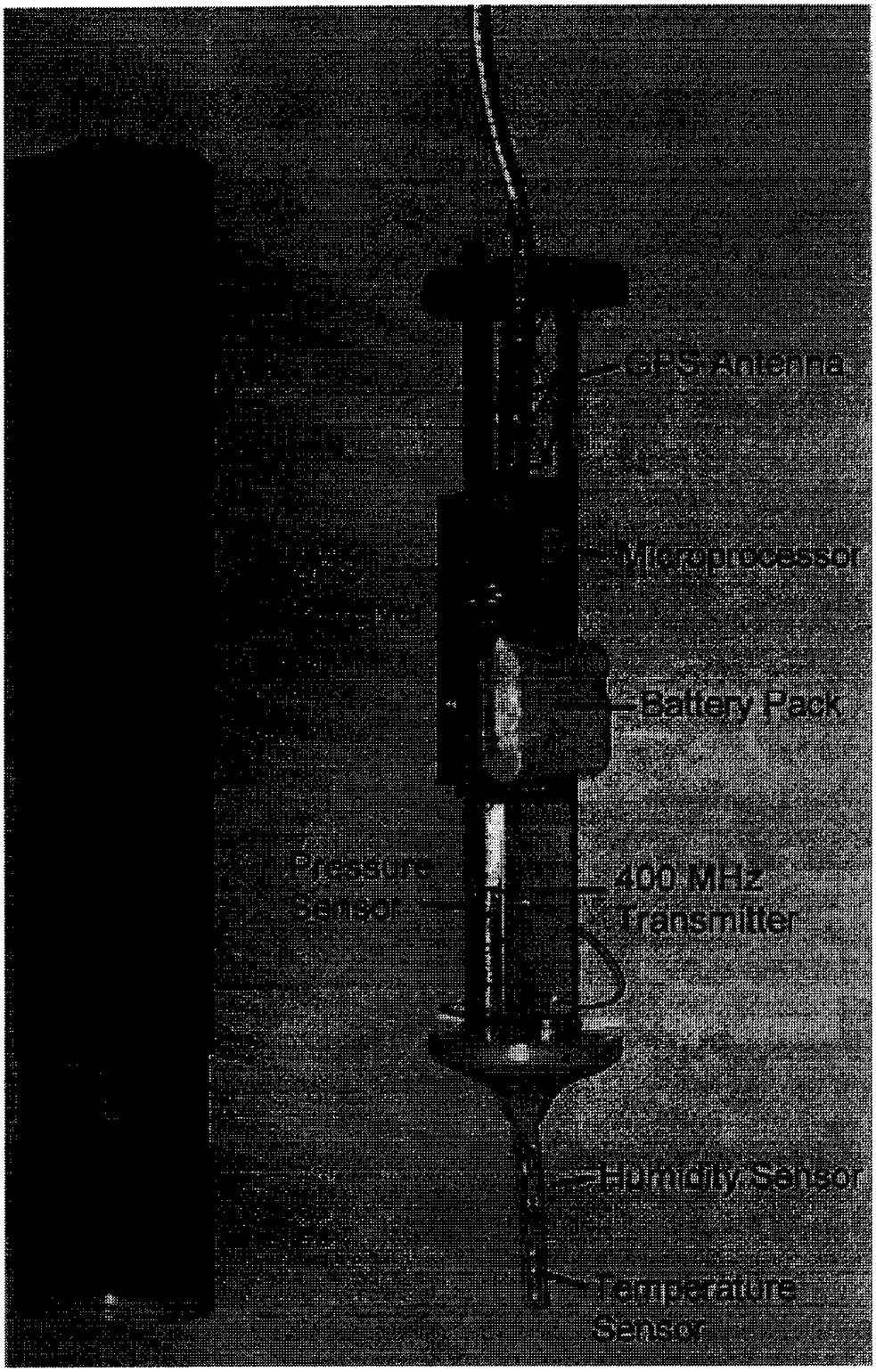

Figure 2.2: GPS dropwindsonde and interval view. From Hock and Franklin (1999).

- Deployment at airspeeds up to 175 m/s
- Telemetry out to a range of 325 km
- Descent time approximately 12 minutes from 12 km
- Sensor measurement rate of 2 Hz

NCAR implemented these requirements by developing the Airborne Vertical Atmospheric Profiling System (AVAPS). It is system that consists of the hardware and software residing on the aircraft, whether it is the G-IV or the P-3s, that is responsible for receiving the data from the dropsonde, determining the sonde motion from the retransmitted GPS doppler frequencies, and then storing the motion and PTH data in a database. It should be noted that four GPS satellites are required for accurate three-dimensional positioning, and consequently, for wind computation. (Kaisti 1995; Saarnimo 1998). However, vertical wind speeds can be determined with less than 4 GPS satellite fixes.

Table 2.3: Typical fall times for the NCAR GPS dropsonde. From Hock and Franklin (1999).

Pressure (mb)	Fall time (min)
850	2.0
700	4.0
500	7.0
400	9.0
300	10.5
250	11.5
200	12.5
150	13.5
100	14.5

The other design specifications were met by either the design of the instrument by NCAR or the performance capabilities of the sensor packages. NCAR's design of the GPS dropsonde resulted in a descent time of about 12 minutes from 12 km (Table 2.3). This fast fall allows the dropsondes to be within the 325 km tracking range. It also helps when rapid launches of dropsondes are needed, because AVAPS can only track 4 dropsondes at any particular time. The sensors were manufactured to NCAR specifications by Vaisala, a Finnish company. Table 2.4

shows that the measurement of pressure, temperature, wind, and humidity are very precise, perform well over a wide range of atmospheric conditions, and have small measurement error.

Table 2.4: Dropwindsonde Sensor Specifications. Accuracy refers to standard deviation of two successive calibrations. From Hock and Franklin (1999).

Range	Accuracy	Resolution
1060-20 mb	0.5 mb	0.1 mb
-90 to + 40°C	0.2°C	0.1°C
0% - 100%	2%	0.1%
0 - 150 m s^{-1}	0.5 m s^{-1}	0.1 m s^{-1}

2.3 Dropwindsonde Accuracy Improvements

The new dropwindsonde is more technically advanced than previous generations of Omega and Loran navigation based dropwindsondes. One significant difference between the GPS dropwindsonde and previous dropwindsondes is its high fall rate. Omega dropwindsondes descended at a rate of about 25mb/min or about 300m/minute. GPS dropwindsondes fall at a rate of about 600m/minute. The high fall rate, coupled with AVAPS capability to monitor up to 4 dropwindsones simultaneously, as opposed to only 3 Omega dropwindsondes using OWDS, provides excellent spatial (horizontal) resolution (Hock 1998). Perhaps the biggest improvement is that wind measurements are taken twice every second as opposed to every 60 seconds for Loran or even 240 seconds for Omega sondes (Hock 1998). Table 2.5 shows the accuracies of the three navigation systems. It is should be obvious that GPS wind-finding provides unpredented accuracy and resolution. The vertical wind resolution is roughly 100 times better than all previous dropsondes and has an improved accuracy by a factor of four (Hock 1998).

Table 2.5: Accuracies of Navigation Systems (Lally, et al. 1989) .

Navigation System	Absolute Accuracy (m)	Differential Accuracy (m)	Wind Accuracy	Measurement Time (Ave)
Omega	2000	200	1-2 m/s	2-3 min
Loran	200	20	1 m/s	30s
GPS	20	<1	10 cm/s	1s

2.4 Summary

The GPS dropwindsonde provides the most accurate and highest resolution sensor package ever made. Its use provides unprecedented accurate observations to examine the inner core thermodynamic and kinematic structure of tropical storms and hurricanes. It should be noted that the results that follow depend on the accuracies referenced in this chapter.

Chapter 3

DATA

3.1 Data Sets

This project used several datasets that are outlined below. The datasets fell into two areas of interest. First is the meteorological data observed by the dropwindsondes as they were launched from flight level. This data set will be referred to as the GPS dropwindsonde data set. The second area of interest deals with storm center positioning. The best-track and two-minute databases were used to determine the most accurate storm center fix in relation to each dropwindsonde launch. Note the following analysis differs from other hurricane research work in that the vertical as opposed to the horizontal view is stressed. This is due to the fact that no flight-level data has been processed for these storms at this time.

3.1.1 GPS Dropwindsonde Data Set

The primary data source for this project was the individual dropwindsonde data files maintained by HRD. This study concentrated on the dropwindsondes launched in and around 6 storms that reached hurricane status during 1997 and 1998. A total of 36 missions were flown into these 6 hurricanes. Table 3.1 lists the storm, mission, aircraft, flight-level where the dropwindsondes were dropped, and the total amount of sondes released on each mission. The N designation denotes G-IV flights where flight level lies around 150 to 200 mb. These missions are the synoptic surveillance flights that primarily cover the periphery of the tropical storms. The H and I flights are performed by the P-3s from the 600 mb level on average. These flights penetrate the inner-core and the storm center.

For these 6 storms that reached hurricane status, a total of 972 dropwindsondes were launched. With the help of the two-minute data, 673 dropwindsondes were navigated from storm

Table 3.1 Storm Mission Data for the 6 Hurricanes from the 1997 and 1998 seasons.

Storm	Date	Aircraft	Drop Pressure (mb)	Sondes Dropped	Storm Total
Guillermo	8/1/1997	I (43)	500	5	
Guillermo	8/2/1997	I (43)	500	39	
Guillermo	8/3/1997	H (42)	700	10	
Guillermo	8/3/1997	I (43)	500	38	
					92
Erika	9/4/1997	N (49)	150	30	
Erika	9/5/1997	I (43)	450	20	
Erika	9/6/1997	N (49)	150	29	
Erika	9/7/1997	I (43)	550	39	
Erika	9/8/1997	I (43)	750	31	
					149
Bonnie	8/20/1998	H (42)	500	20	
Bonnie	8/20/1998	I (43)	500	16	
Bonnie	8/20/1998	N (49)	150	31	
Bonnie	8/21/1998	H (42)	500	24	
Bonnie	8/21/1998	N (49)	150	27	
Bonnie	8/23/1998	H (42)	500	32	
Bonnie	8/23/1998	I (43)	600	17	
Bonnie	8/23/1998	N (49)	150	28	
Bonnie	8/24/1998	H (42)	600	28	
Bonnie	08/24/98	N (49)	150	30	
Bonnie	08/26/98	H (42)	600	47	
Bonnie	08/26/98	I (43)	800	41	
Bonnie	08/28/98	N (49)	200	30	
					371
Danielle	08/29/98	H (42)	650	22	
Danielle	08/29/98	I (43)	500	38	
Danielle	08/29/98	N (49)	200	29	
Danielle	08/30/98	H (42)	550	21	
Danielle	08/30/98	I (43)	750	29	
Danielle	08/30/98	N (49)	200	34	
Danielle	09/01/98	N (49)	200	27	
					200
Georges	09/16/98	N (49)	200	28	
Georges	09/18/98	H (42)	450	4	
Georges	09/18/98	N (49)	200	14	
Georges	09/19/98	H (42)	600	32	
Georges	09/19/98	I (43)	600	24	
Georges	09/19/98	N (49)	200	27	
					129
Mitch	10/27/1998	I (43)	700	31	
					31
		Total Sondes Dropped:		972	972

center. With the navigation completed, the radial and tangential winds were then computed . Table 3.2 further breaks down this set into various regions of the storm.

Table 3.2: Hurricane dropwindsonde drops by location from 1997 and 1998 seasons. Outer-Core represents sondes outside the eye and eyewall. Intersection represents sondes released into the eye but enter the eyewall region during their descent.

Location	Eyewall Drops
Eye	36
Eyewall	92
Outer Core (within 120Km of storm center)	543 (162)
Intersection	2
	Total: 673

Table 3.3 highlights the number of eyewall drops by storm while table 3.4 lists the number of eye drops by storm.

Table 3.3: Hurricane eyewall dropwindsonde drops by storm from 1997 and 1998 seasons.

Storm	Eyewall Drops
Bonnie	27
Danielle	17
Erika	14
Georges	12
Guillermo	6
Mitch	16
	Total: 92

Table 3.4: Hurricane eye dropwindsonde drops by storm from 1997 and 1998 seasons.

Storm	Eye Drops
Bonnie	11
Danielle	7
Erika	2
Georges	2
Guillermo	8
Mitch	5
	Total: 36

Taken in context of the 972 total drops into these storms, eyewall drops accounted for 10%, eye drops accounted for only 4%, and inner-core drops (within 120KM of storm center) accounted for 17% of the total.

Appendix A contains a sample dropwindsonde data file and a description on how to interpret it. It should be noted that the important parameters deal with three meteorological areas of interest; thermodynamics, kinematics (wind speed and direction), and location in the horizontal and the vertical. Note that some meteorological quantities need to be derived from other given quantities from the data file. For example, the data file gives relative humidity as the only measure of the moisture content. In order to determine dew point, an algorithm was used to derive it from temperature and relative humidity. Other derived quantities included potential temperature and equivalent potential temperature.

Since the GPS dropwindsonde data files did not provide all the information required, a database was created and a program was written to process all the data files, calculate the missing derived quantities, and then store the results in the database. Storing all the data in a database offers many advantages. First, instead of handling hundreds or perhaps in the future, thousands of files, only one database needs to be referred to for the information. In addition, database management systems provide sophisticated tools and a language that can be exploited quickly and efficiently. As such, the overall goal was to get the data, process it, input it into the database, and then perform the research.

3.2. Best-Track Data

HRD also maintains a hurricane track and intensity summary for each storm that is known as the "best-track" database. It is termed "best" because it uses a combination of all reliable existing track and intensity observations during post-season analysis to determine the most accurate track and intensities for each storm (Eastin 1999). The best-track data contains the storm center location in terms of latitude and longitude , storm motion given in direction and speed, maximum sustained wind speed, and minimum sea-level pressure (MSLP). Generally, the storm fixes are given in only in 3 to 6 hour intervals, making this set of data not of the best quality in terms of time resolution for determining accurate inner core winds in cylindrical coordinates. However, this

data does provide the continuity day over day for storm tracking and best estimate of the hurricane track and intensity. Figure 3.1 shows the track of hurricane Guillermo from the 1997 season in the eastern Pacific while figure 3.2 shows the tracks of Atlantic hurricanes consisting of Erika from the 1997 season and hurricanes Bonnie, Danielle, Erika, Georges, and Mitch from the 1998 season. The locations marked by an X represent an estimate of where the aircraft mission penetrated these storms. Figures 3.3-3.8 shows graphs by individual storm in terms of two intensity parameters; minimum sea level pressure (MSLP) and maximum sustained wind speed. Additionally, the duration of all investigation flights are also over-plotted.

3.3 Two-minute Data

The two-minute storm center database is more accurate than the best-track database. This data set contains two-minute storm center fixes derived from the flight of the aircraft during its mission. The two-minute data is computed at HRD using a cubic spline method to interpolate between storm center fixes (Willoughby and Chelmow 1982). This data set only gives storm center in terms of latitude and longitude, but this data is critical in determining accurate radial wind and tangential wind profiles. Figure 3.9 shows the result of using GPS dropwindsondes with the two-minute data where the individual dropwindsondes can be navigated to storm relative center position.

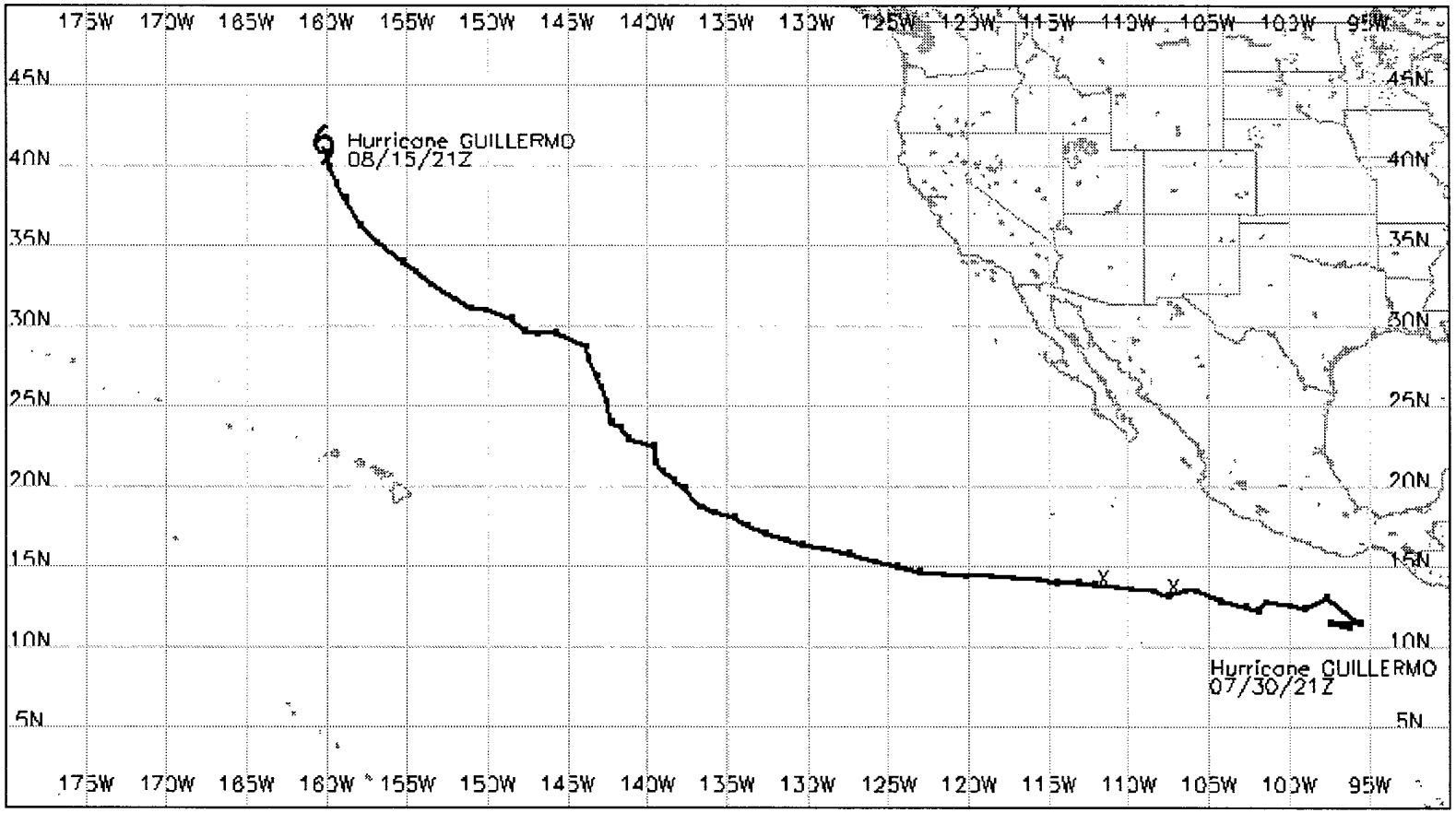

Figure 3.1: Track of Eastern Pacific Hurricane Guillermo (1997). Xs denote inner-core aircraft mission flights.

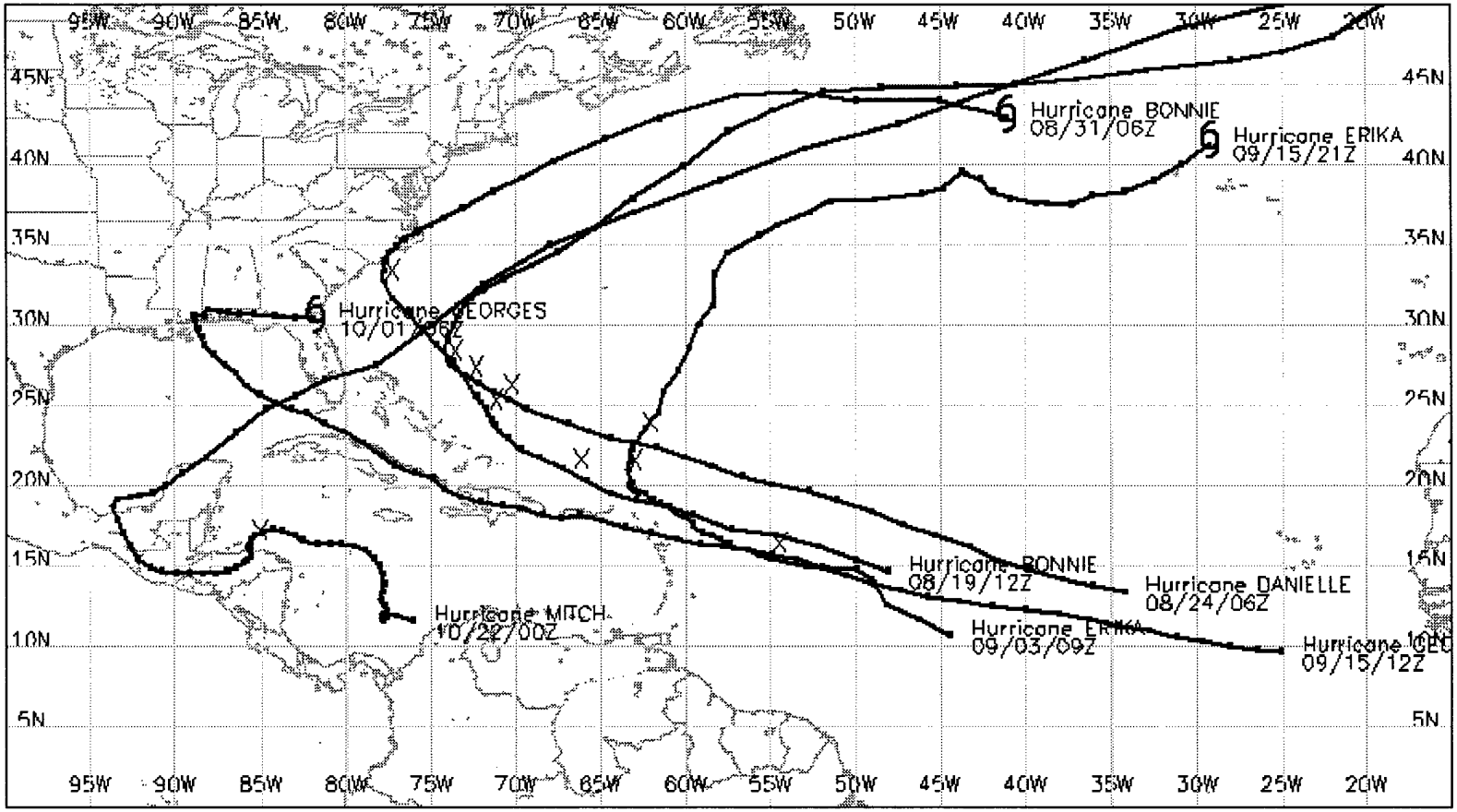

Figure 3.2: Tracks of Atlantic Hurricanes from the 1997 (Erika) and 1998 (Bonnie, Danielle, Erika, Georges, and Mitch seasons.). Xs denote inner-core aircraft mission flights.

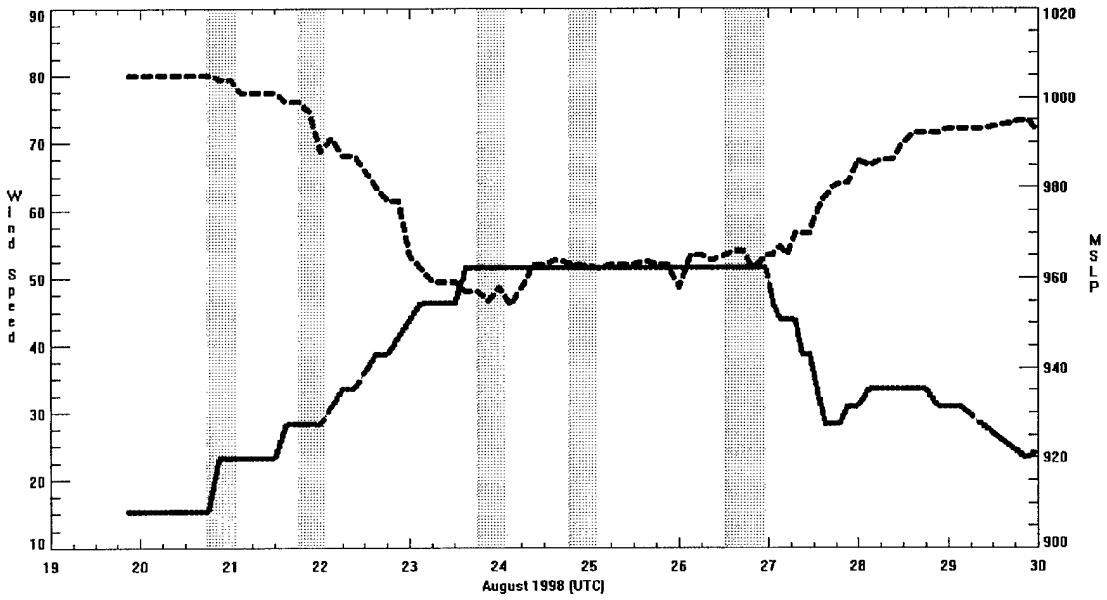

Figure 3.3: Hurricane Bonnie best track maximum sustained wind speed (m/s (solid)) and MSLP (mb (dashed)). Gray bars denote aircraft mission over flight times.

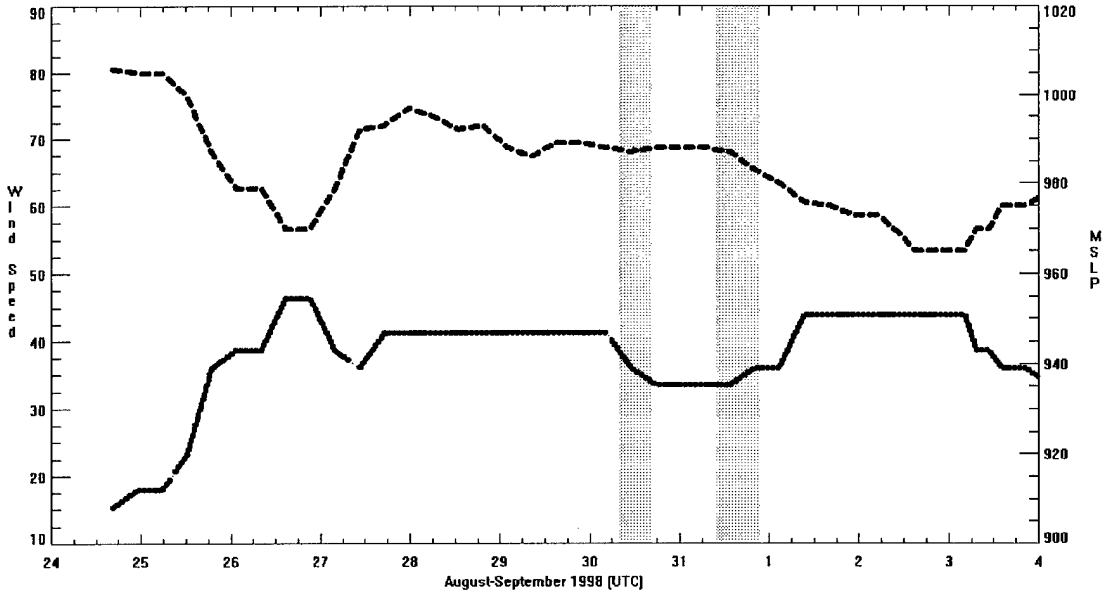

Figure 3.4: Hurricane Danielle best track maximum sustained wind speed (m/s (solid)) and MSLP (mb (dashed)). Gray bars denote aircraft mission over flight times.

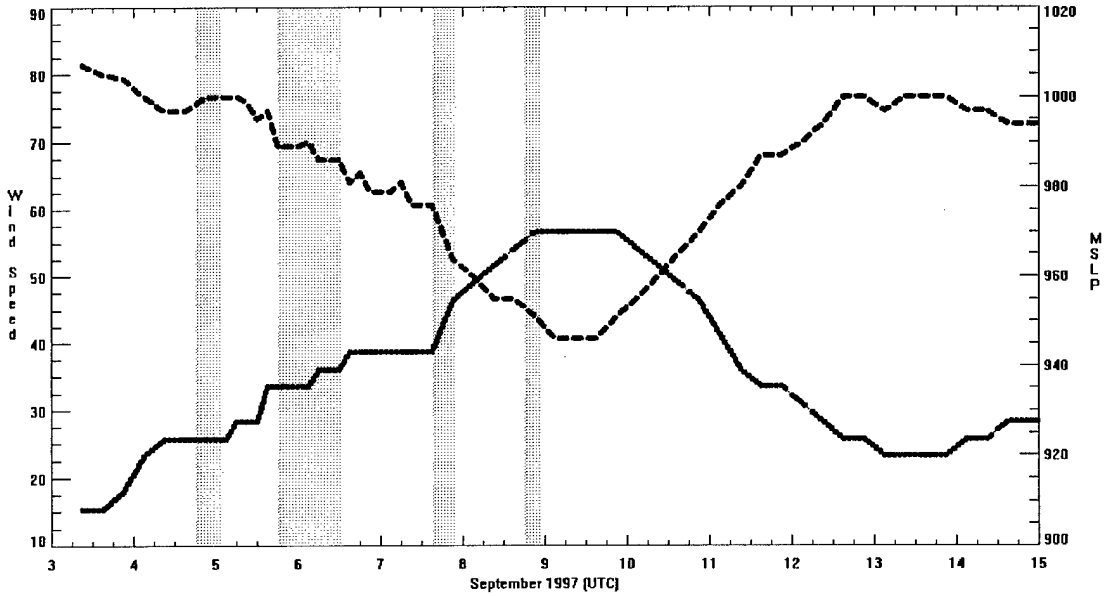

Figure 3.5: Hurricane Erika best track maximum sustained wind speed (m/s (solid)) and MSLP (mb (dashed)). Gray bars denote aircraft mission over flight times.

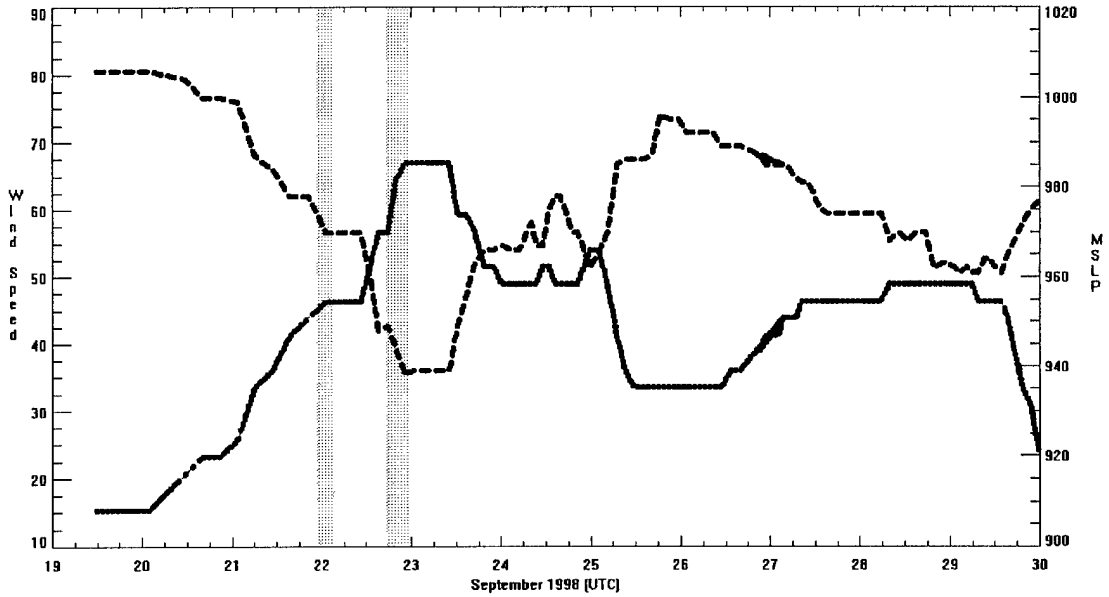

Figure 3.6: Hurricane Georges best track maximum sustained wind speed (m/s (solid)) and MSLP (mb (dashed)). Gray bars denote aircraft mission over flight times.

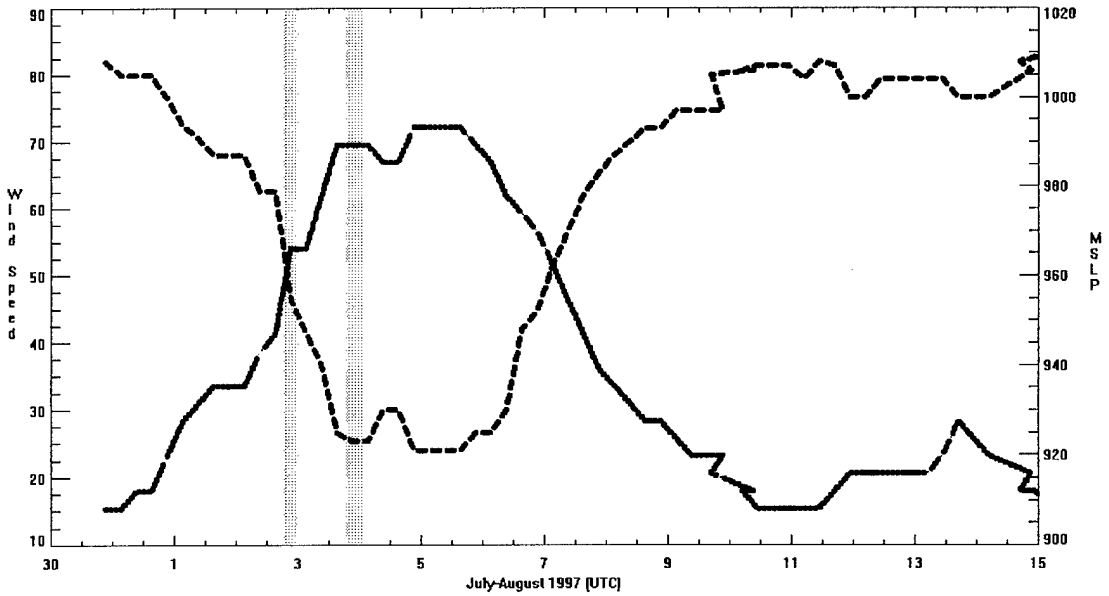

Figure 3.7: Hurricane Guillermo best track maximum sustained wind speed (m/s (solid)) and MSLP (mb (dashed)). Gray bars denote aircraft mission over flight times.

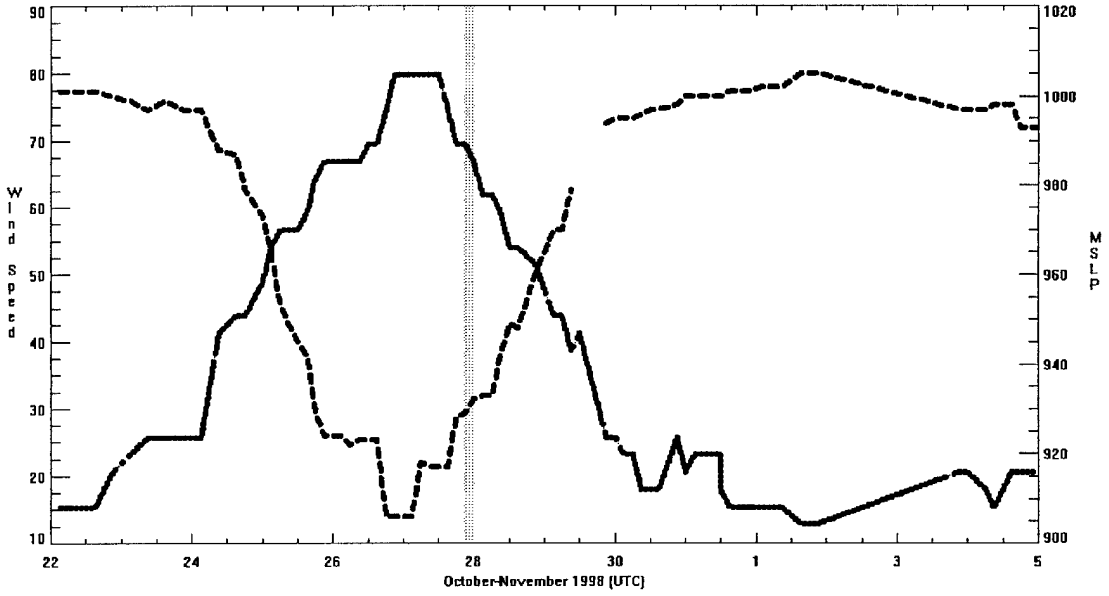

Figure 3.8: Hurricane Mitch best track maximum sustained wind speed (m/s (solid)) and MSLP (mb (dashed)). Gray bars denote aircraft mission over flight times.

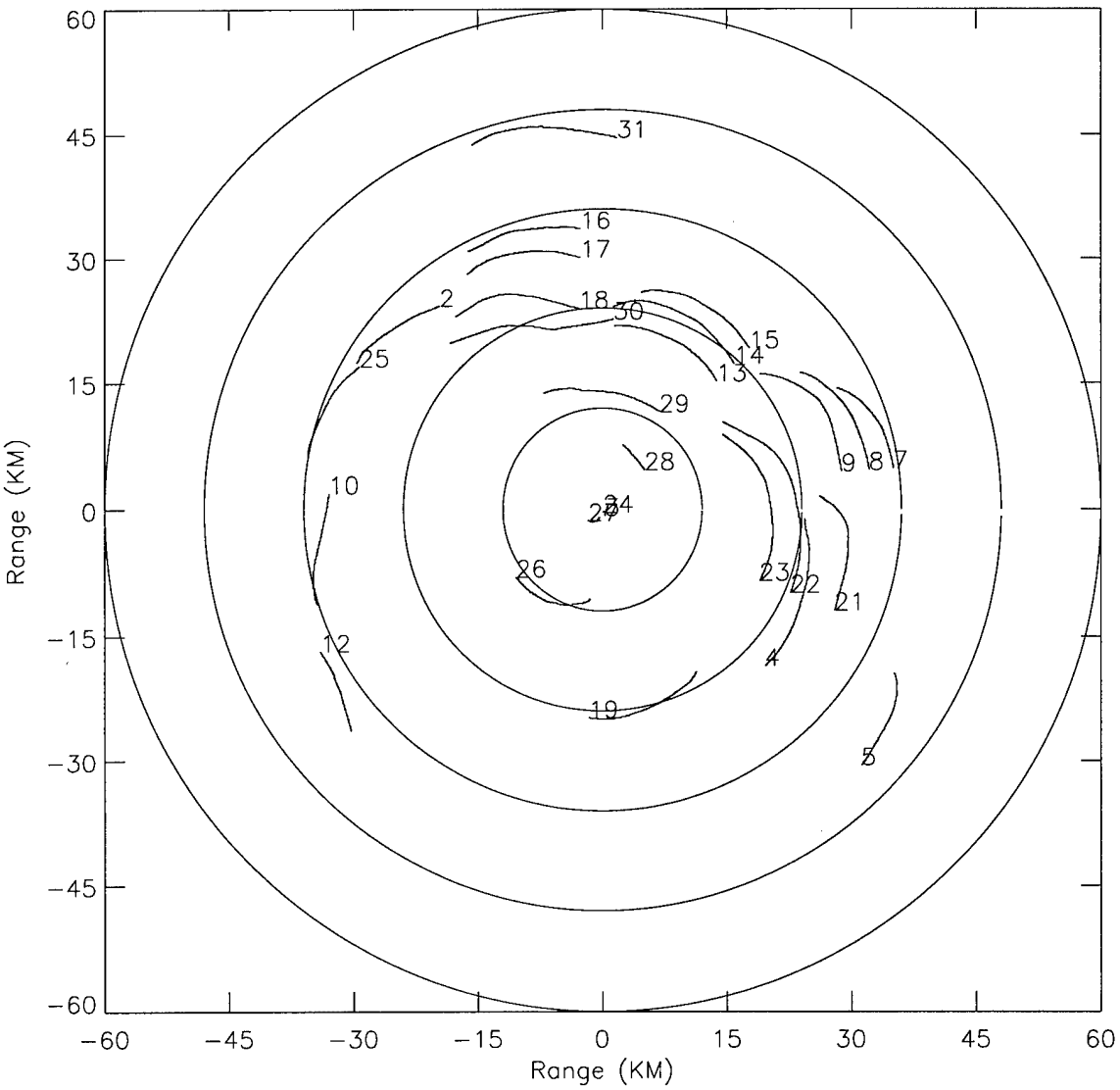

Figure 3.9: Polar plot of dropwindsondes launched into Hurricane Mitch on October 10th, 1998. Rings are at 12km increments. Numbers represent the order of the dropsonde launches.

Chapter 4

RADIAL AND TANGENTIAL WIND ANALYSIS

4.1 Radial and Tangential Wind Derivation

The dropwindsonde data set includes the components of u and v and total wind speed (Appendix A). In order to determine radial and tangential winds another data set was needed. This second data set consisted of the two-minute storm center fixes determined from the careful navigation of the flights. This data set gives the storm center latitude and longitude every two minutes for most of the duration of the flight. From this data set alone, most of the drop trajectories could be related to the storm center. For times when drops were made but no corresponding storm center fix was available from the two-minute data, the last storm center fix and the nearest best track data entry was used to interpolate the position corresponding to the drop time. For the inner core drops this navigation problem was not an issue because the two-minute data covered these drops. For drops outside the core, this procedure was necessary in order to derive the radial and tangential winds.

With the above procedural steps were taken, the range, radial wind, and tangential wind were computed in the following fashion: First, storm center latitude and longitude were interpolated from the two-minute data matching the time of the dropwindsonde launch. Second, the sondes coordinates were used in conjunction with the storm center coordinates to determine range, azimuth, radial wind, and tangential wind. This process was repeated for each record in each dropsonde data file.

Following the above computations, a storm relative coordinate system was used to display the actual drops within the core of the storms. Figure 3.9 showed one of the storm relative dropwindsonde drop location plots. The purpose of the storm relative coordinate system is to eliminate the time factor. If the mission covered most of the inner core, we are able to view a plot of

all data as a snapshot of the storm where all the drops can be taken as being at positions in relation to storm center.

4.2 Radial Wind Determination From Friction

Derivation of the radial wind that would be attributed to friction was carried out in the following manner. First a cylindrical coordinate system was used along with the assumption that the storms were symmetrical in relation to this system. We may view the change of the tangential wind as a function of two terms:

$$\partial Vt / \partial t = Generation + Dissipation \tag{4.1}$$

Equation 4.1 may be rewritten for these two terms to arrive at equation 4.2.

$$\partial Vt / \partial t = -Vr\zeta r + \vec{F} \tag{4.2}$$

Additionally, assuming that the Coriolis parameter is much smaller than the relative vorticity in the inner-region we can state that $\zeta_a \approx \zeta_r$. Where ζr is given in equation 4.3.

$$\zeta r = Vt / r + \partial Vt / \partial r \tag{4.3}$$

If we assume that we are at the radius of maximum winds then the shear of the vorticity drops out and relative vorticity becomes and we arrive at a form of the tangential wind equation (4.5).

$$\zeta r = Vt / r \tag{4.4}$$

$$\partial Vt / \partial t = -VrVt / r + \vec{F} \tag{4.5}$$

The frictional dissipation can be viewed as the shear of the surface stress over the depth of the boundary layer (Equation 4.6). We can approximate equation 4.6 using the bulk formula shown in equation 4.7.

$$\vec{F} = \partial \tau_z / \rho \partial z \tag{4.6}$$

$$\vec{F} \approx C_d Vt^2 / \Delta Z \tag{4.7}$$

If we now assume steady state then the change in the tangential wind with time is zero. Substituting equation 4.7 into 4.5 we arrive at equation 4.8.

$$0 = VrVt / r + C_d Vt^2 / \Delta Z \tag{4.8}$$

Upon rearrangement we arrive at the radial wind determined from frictional forcing in equation 4.9 where the radius and tangential wind is averaged over the depth of the boundary layer.

$$Vr = \bar{r} C_d \bar{V}t / \Delta Z \tag{4.9}$$

Additionally, equation 4.9 can be rearranged to solve for the drag coefficient (C_d).

$$C_d = Vr\Delta Z / rVt \tag{4.10}$$

With equation 4.9 in hand, determination of the frictionally induced radial wind was carried out for each dropsonde with the assumption that the drag coefficient (C_d) was 2 X 10^{-3} and that the boundary layer ΔZ was either 500 or 1000 meters. The drag coefficient was chosen after Rosenthal's (1975) equation for the drag coefficient based on equation 4.11.

$$C_d = 1.1x10^{-3} + 4x10^{-5}V \tag{4.11}$$

The average radius and tangential wind were taken from dropsonde data that fell into the region of the surface and the 500 or 1000-meter level.

4.3 Comparison of Observed Radial Winds to Frictionally Induced Radial Winds

The dropsonde data in the eyewall region consisted of 94 sondes. Overall, 83% of the inner core dropwindsondes had inflow winds within the boundary layer. Table 4.1 breaks down the ratio of the observed radial wind inflow to that of frictionally induced radial inflow into 4 different quadrants when the boundary layer was taken to be 500 meters.

Table 4.1: Ratio of Actual Average Radial Wind to that computed from friction for a 500 meter boundary layer (Eyewall drops).

	Average Radius	
Vt	<50.0 Km	>50.0Km
>40.0 m/s	2.2	0.8
<40.0 m/s	1.7	0.7

The strongest tangential winds with average radiuses of less that 50 km reported the largest deviation from friction. At larger radius and for both strong and weak winds the observed radial winds match closely that specified by friction alone with the assumed drag coefficient. For winds

less than 40 m/s and radius less than 50 km, the ratio was not as large, but significant in that the observed radial winds were greater than those due to friction. The result is that the smaller the eyewall the greater the radial inflow over what surface friction would dictate.

Table 4.2 presents the same data as seen in table 4.1, but with the assumption that the depth of the boundary layer was 1000 meters. As will be shown in the next section, from the vertical profiles of the radial wind, 1000 meters represents the average depth of the inflow layer. Using this finding the boundary layer was taken to be 1000 meters. Of course a study of the depth of a well-mixed thermodynamic parameter, such as specific humidity, could have been researched to determine the depth of the boundary layer. Powell et al. (1999) looked at the depth of the boundary layer as measured from the dropsondes within hurricane Guillermo and found that specific humidity and potential temperature (θ) were well mixed up to the 500 meter level. However, only one cyclone was analyzed; more work needs to be done to say that 500 meters is the depth of the boundary layer. In any case, this depth could be extended up to 1000 meters without much error. With this in mind, the results are nearly identical for both boundary layers. Again, the smaller the eye and the greater the storm intensity, the greater the radial inflow over that dictated from friction.

Table 4.2: Ratio of Actual Average Radial Wind to that computed from friction for a 1000 meter boundary layer (Eyewall drops).

	Average Radius	
Vt	<50.0 Km	>50.0Km
>40.0 m/s	2.4	0.8
<40.0 m/s	2.2	1.1

For all storms the overall ratio was 2.1 to 1 of actual radial wind inflow over that computed from friction when the boundary layer was taken to be that of 500 meters. When the boundary was chosen to be 1000 meters, the results were nearly identical where the overall ratio was 2.2 to 1 of actual radial wind inflow over that computed from friction.

The outer-core was also analyzed to determine if the observed radial wind significantly differed from that of friction. The dropsondes used in this region resided outside the eyewall region,

but within 120km of storm center. In the outer region the ratio was 0.9 to 1 of actual radial wind inflow over that computed from friction when the boundary layer was 500 meters. With the boundary layer of 1000 meters the ratio was 1.1 to 1. Therefore, in this region the radial wind is balanced by friction.

Table 4.3: Ratio of Actual Average Radial (Vr) Wind to that computed due to friction by storm and mission.

Storm	Intensity	Mission	Drops	Eyewall Ratio	Outer Ratio	Eyewall/Outer Ratio
Guillermo	5	19970803H	6	1.9	0.9	2.2
Erika	1	19970907I	8	0.7	1.7	0.4
Erika	3	19970908I	6	2.4	0.5	4.9
Bonnie	3	19980826H	7	0.8	1.1	0.8
Bonnie	3	19980826I	17	0.9	1.4	0.6
Danielle	2	19980830I	17	1.5	0.6	2.4
Georges	3-4	19980919H	6	3.8	0.7	5.1
Georges	3-4	19980919I	6	3.1	0.7	4.4
Mitch	5	19981027I	16	4.2	1.8	2.3
			Average:	2.1	1.0	2.6

In addition to eyewall and outer-core analyses, the radial wind was also looked at on an individual storm basis. Table 4.3 shows that the magnitude of the ratio of observed radial winds to friction induced varies by storm and intensity. Generally, the stronger the intensity of the storm as measured by the Safford-Simpson (1974) scale, the larger the ratio. Note that for the outer region of the storms the ratio is not as variable as in the eyewall region and again the ratio approximates 1 to 1 over all storms. The ratios for Erika on the 7th of September and for hurricane Bonnie in the eyewall are significantly less than the other storms for the same intensity. It is hypothesized that hurricane Bonnie was undergoing vertical shear at this time as evidenced by figure 3.3, and this disrupted the storm from intensifying. This resulted in the lower ratio. Hurricane Erika on the 7th was just beginning a period of intensification as seen from figure 3.5. Only 3 of the 8-eyewall sondes dropped at this time report inward radial wind profiles over the 1000-meter inflow layer. It is hypothesized that the storm was still getting organized when the dropwindsondes were launched as seen from figures 4.1 and 4.2, and that this lead to the reduced ratio value.

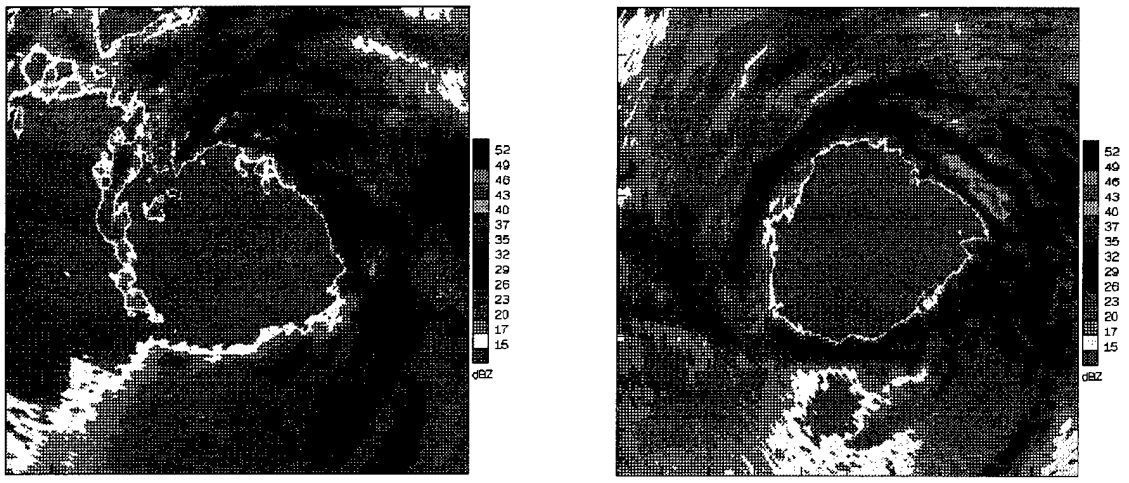

Figures 4.1 and 4.2: Hurricane Erika on 7 September 1997 at 1725Z (left) and 1915Z (right). Note the rapid development over this short time interval. Reflectivities given in dBZ

4.4 Role of the Vertical Gradient of the Radial Wind in Determining Storm Intensity

Figure 4.3 shows the vertical profile of the radial wind based on a 10 meter average over all eyewall sondes and all outer core sondes. Notice from the plot the eyewall radial wind is about a factor of 2.5 greater from that given from the outer regions. For comparison the tangential wind profiles for the eyewall and the outer-core sondes are plotted in figure 4.4. From this plot the tangential wind in the eyewall exceeds up to 5 times that of the outer-core. Returning to the radial wind profiles, note that both the eyewall and the outer core plots of the radial wind suggest the depth of the inflow layer is around 1000 meters. This accounts for the recalculation of the average radial wind observed from friction using 1000 meters as the depth of the boundary layer. Additionally, figures 4.5-4.10 show the vertical profile of the radial wind for all 6 hurricanes from the 1997 and 1998 seasons based on 10-meter averaging. The results generally are the same: Radial wind inflows in the eyewall are approximately twice that over the outer regions.

By using figures 4.5-4.10 the vertical gradient of the radial wind was calculated for all 6 hurricanes to see if this parameter has any connection to the intensity of the storm as based on the Saffir and Simpson (1974) tropical storm intensity scale. Table 4.4 shows that the greater the gradient of the radial wind the stronger the storm as seen from hurricanes Mitch and Guillermo. The category 3 to 4 storms had weaker gradients, while the weakest gradient was seen for the

weakest hurricane--Danielle. Although 6 hurricanes is a very small population these results suggest that the degree of vertical gradient of radial wind is related to the overall storm intensity.

Table 4.4: Vertical gradient of the radial wind corresponding to storm intensity based on the Saffir-Simpson tropical storm intensity scale.

Storm	**Intensity Category**	$\partial Vr / \partial z$ **(m/Km per s)**
Guillermo	5	27
Erika	1-3	15
Bonnie	3	14
Danielle	2	7
Georges	3-4	16
Mitch	5	23

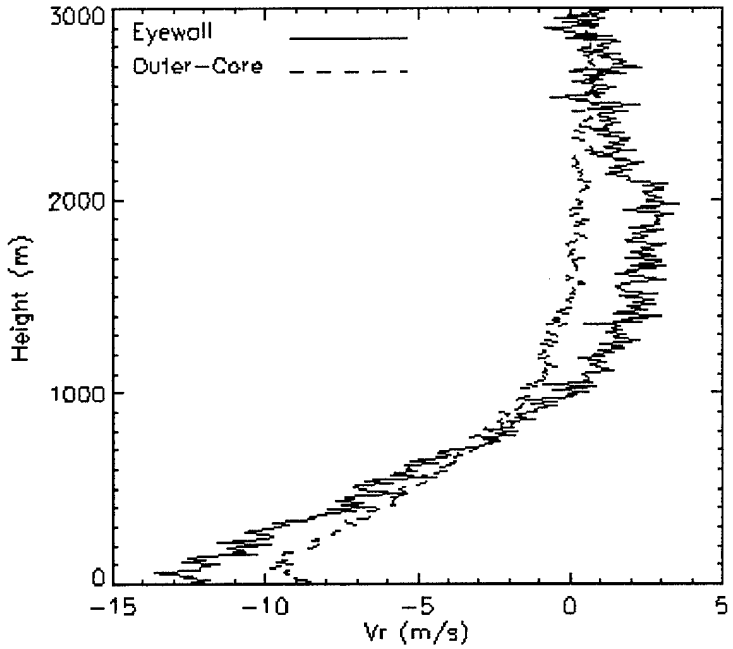

Figure 4.3: Radial Wind inflow plotted versus height for all 6 hurricanes (92 eyewall and 162 outer-core drops). Solid line consists of eyewall drops, while dashed line consists of the outer core drops.

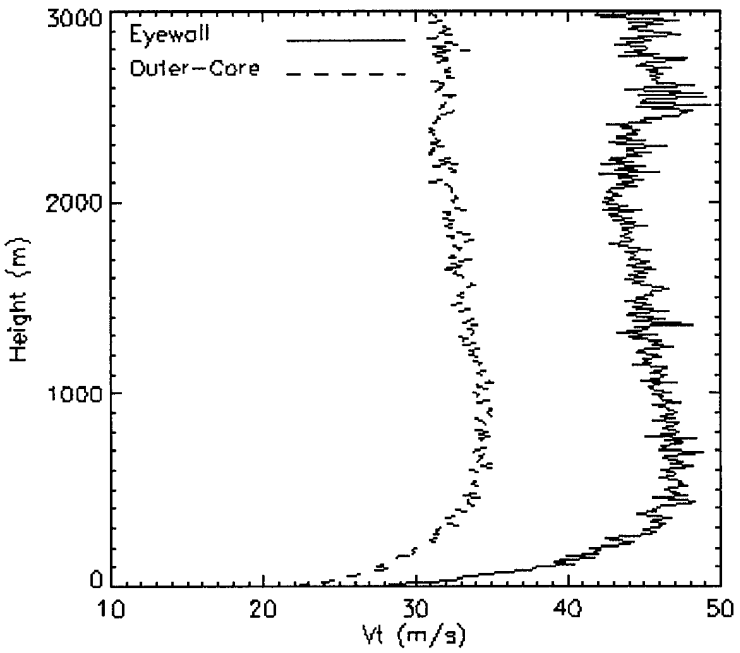

Figure 4.4: Tangential Wind inflow plotted versus height for all 6 hurricanes (92 eyewall and 162 outer-core drops). Solid line consists of eyewall drops, while dashed line consists of the outer core drops.

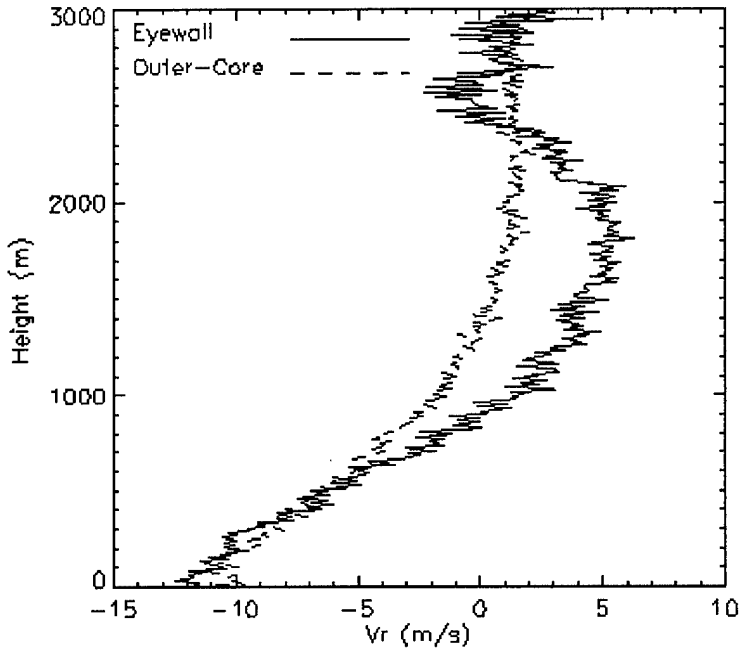

Figure 4.5: Radial Wind inflow plotted versus height for Hurricane Bonnie. Solid line consists of eyewall (27) drops, while dashed line consists of the outer core (64) drops.

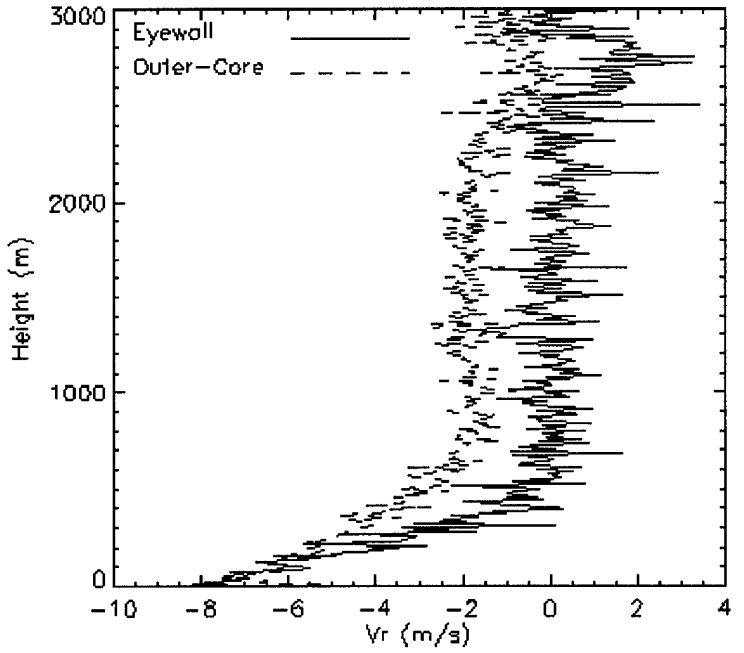

Figure 4.6: Radial Wind inflow plotted versus height for Hurricane Danielle. Solid line consists of eyewall (17) drops, while dashed line consists of the outer core (37) drops.

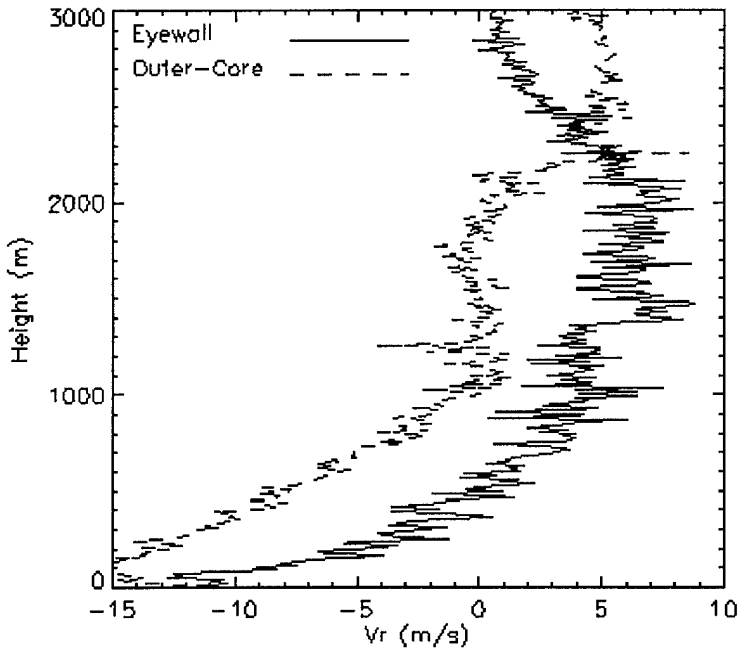

Figure 4.7: Radial Wind inflow plotted versus height for Hurricane Erika. Solid line consists of eyewall (14) drops, while dashed line consists of the outer core (17) drops.

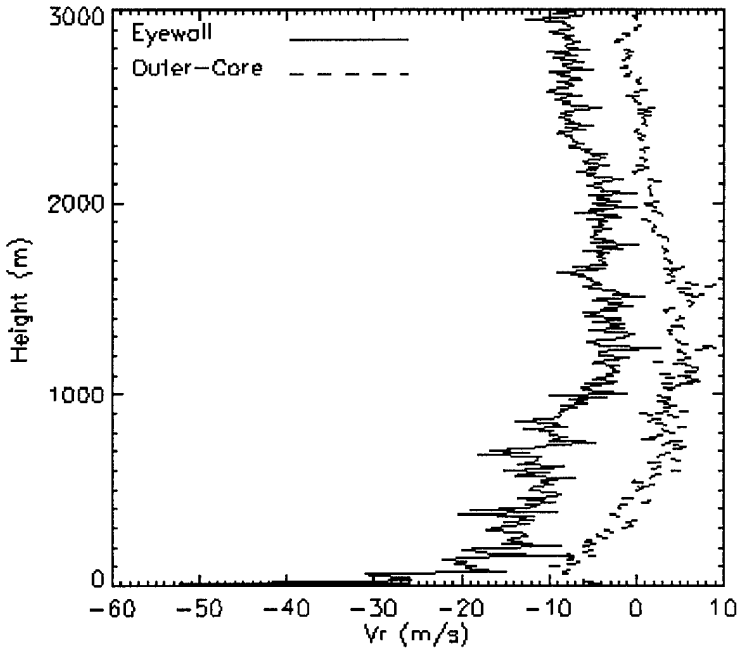

Figure 4.8: Radial Wind inflow plotted versus height for Hurricane Georges. Solid line consists of eyewall (12) drops, while dashed line consists of the outer core (13) drops.

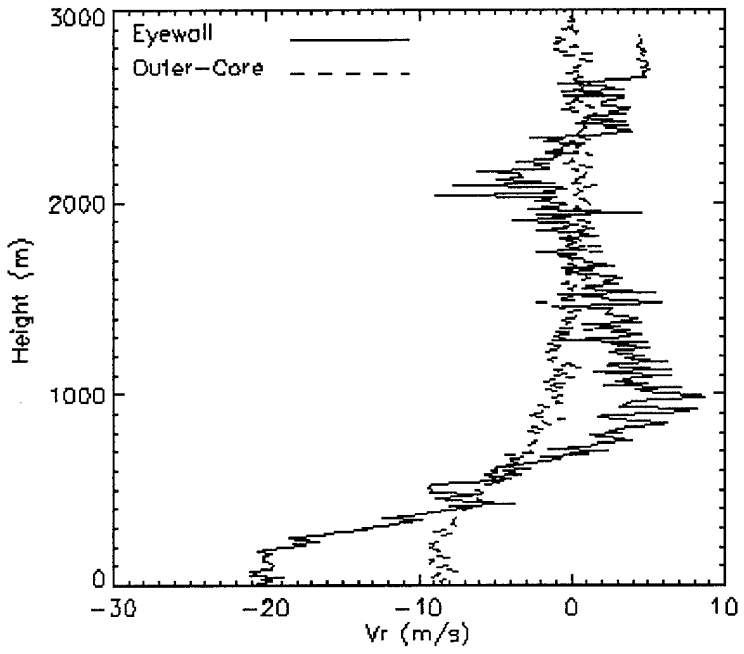

Figure 4.9: Radial Wind inflow plotted versus height for Hurricane Guillermo. Solid line consists of eyewall (6) drops, while dashed line consists of the outer core (25) drops.

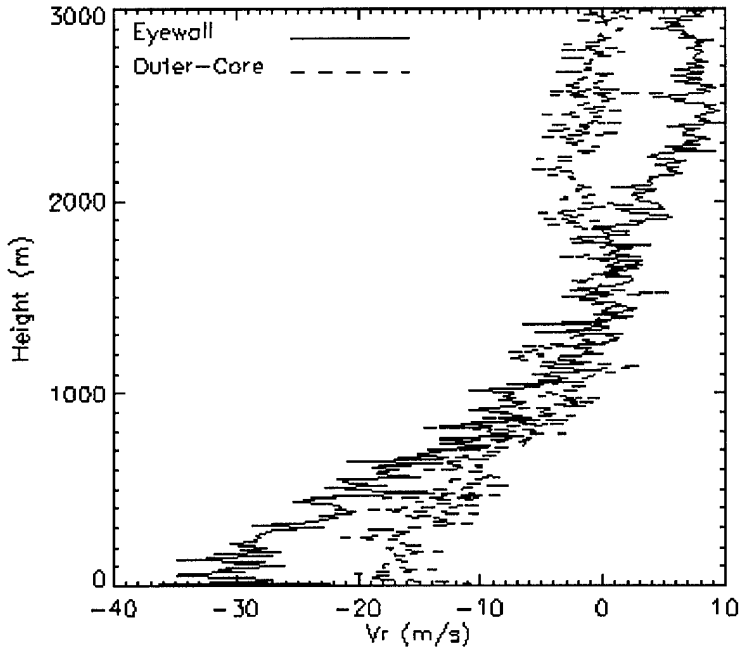

Figure 4.10: Radial Wind inflow plotted versus height for Hurricane Mitch. Solid line consists of eyewall (16) drops, while dashed line consists of the outer core (6) drops.

4.5 Summary

It was shown that the degree of radial inflow within the eyewall region is approximately 2 to 1 over that from friction. It was also shown that in the outer core the observed radial wind closely approximates that of friction. Figure 4.11 shows a schematic of these results. These results suggest that within the eyewall region there is another forcing mechanism responsible for this extra amount of radial inflow. It is hypothesized that this extra forcing is due to buoyancy processes. Future work would do well to address this issue.

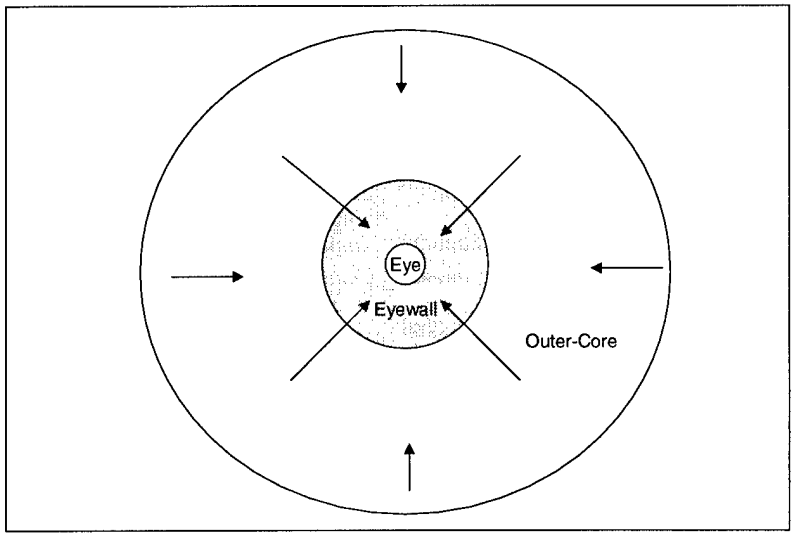

Figure 4.11: Schematic representation of the degree of radial inflow compared two that of friction of the inner core region compared to the outer region of a tropical storm.

Chapter 5

HURRICANE THERMODYNAMICS

An initial look at various thermodynamic parameters was undertaken to get an overall idea of the thermodynamic structure within hurricanes. Dropsonde data was compiled into 3 different regions; eye, eyewall, and outer-core. The eye and eyewall drops were obtained through the use of the catalog files (Appendix A) while the outer core sondes were chosen to be within 120km of storm center. For the 6 hurricanes from the 1997 and 1998 seasons there were 33 eye, 94 eyewall, and 163 sondes that fell into these categories. Figures 5.1 through 5.5 show the results of 10 meter averaging from the surface to 3000 meters in height for the thermodynamic parameters of temperature (t), potential temperature (θ), equivalent potential temperature (θ_e), specific humidity (q), and relative humidity (rh).

5.1 Temperature and Potential Temperature Profiles

Figure 5.1 shows the vertical profiles of temperature for sondes that fell into the eye, eyewall, and outer-core regions of all six hurricanes. It is interesting to note that the eyewall temperatures are cooler than the eye and outer-core at the surface. This is primarily due to evaporative cooling associated with the heavy precipitation in the eyewall region. At higher levels the eye temperature is warmer than the eyewall and outer-core conforming to our understanding that tropical storms are warm-core systems.

Figure 5.2 shows the vertical profiles for potential temperature. All three profiles follow what one would expect from derivation of potential temperature. The parcels are normalized to 1000 mb, and, since the pressure in the eye is lower than under the eyewall region which in turn is lower than the outer-core region, the air parcels in the eyewall have to be taken adiabaticaly down further than the outer-core while the eye air parcels have to be taken down further than in the eyewall region. The result is more adiabatic warming occurs as one approaches the

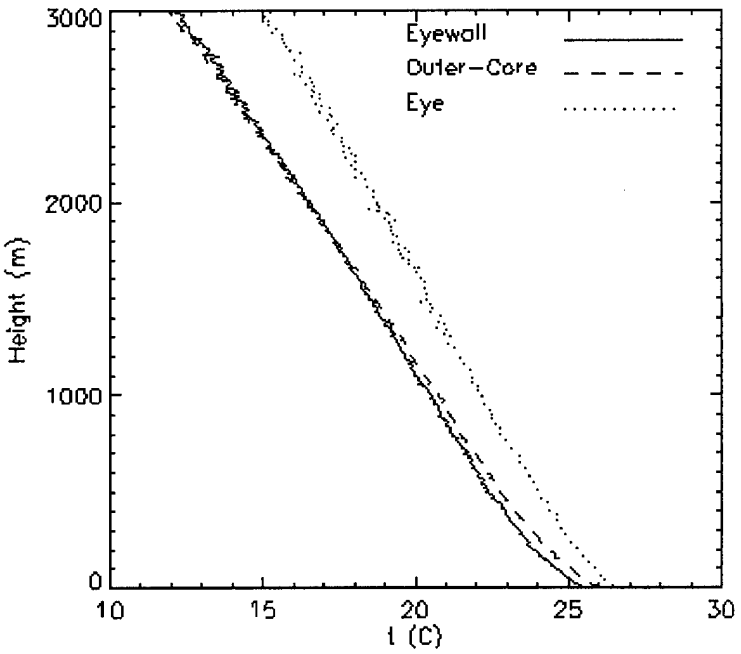

Figure 5.1: Temperature profiles with 10 meter averaging from all 6 hurricanes. Solid line-eyewall (92 sondes), dashed-outer core (163 sondes), and dotted-eye (36 sondes).

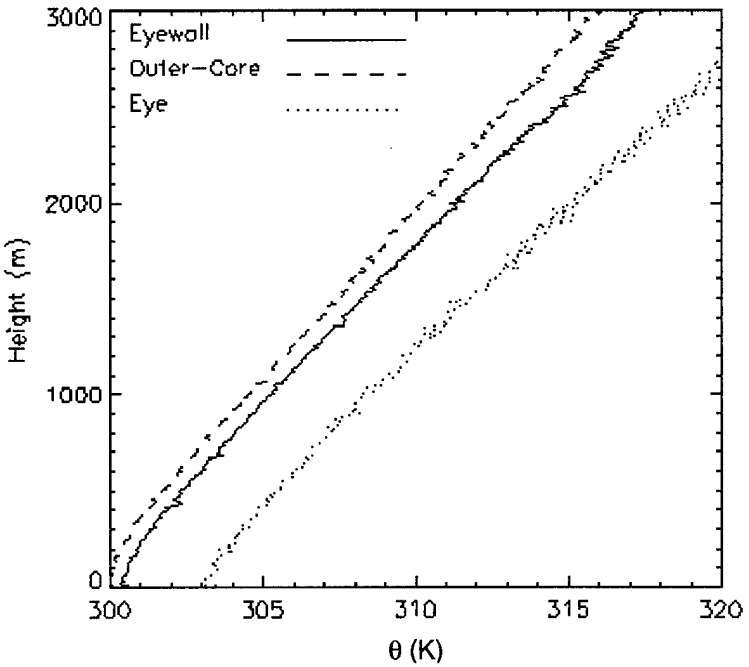

Figure 5.2: Potential temperature profiles with 10 meter averaging from all 6 hurricanes. Solid line-eyewall (92 sondes), dashed-outer core (163 sondes), and dotted-eye (36 sondes).

center of the storm. However, once again we see that the eye potential temperature is greater than the eyewall or outer-core reconfirming our understanding of tropical cyclones as warm core systems.

5.2 Relative Humidity and Specific Humidity Profiles

It is interesting to note from the relative humidity (RH) profile that the RH is high not only in the eyewall, but also in the eye (Figure 5.3). Relative humidity values within the eyewall and the eye are approximately the same up to the 1000-meter level. This suggests some degree of mixing and or inflow into the eye region. The specific humidity profiles (Figure 5.4) show that the moisture content increases approaching the eye of the storm. This is expected due to surface fluxed of heat and moisture.

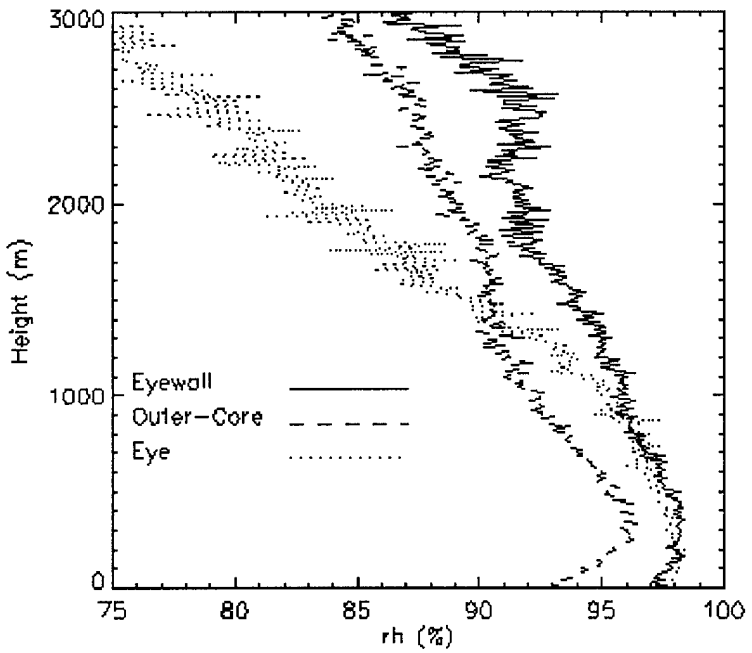

Figure 5.3: Relative humidity profiles with 10-meter averaging from all 6 hurricanes. Solid line-eyewall (92 sondes), dashed-outer core (163 sondes), and dotted-eye (36 sondes).

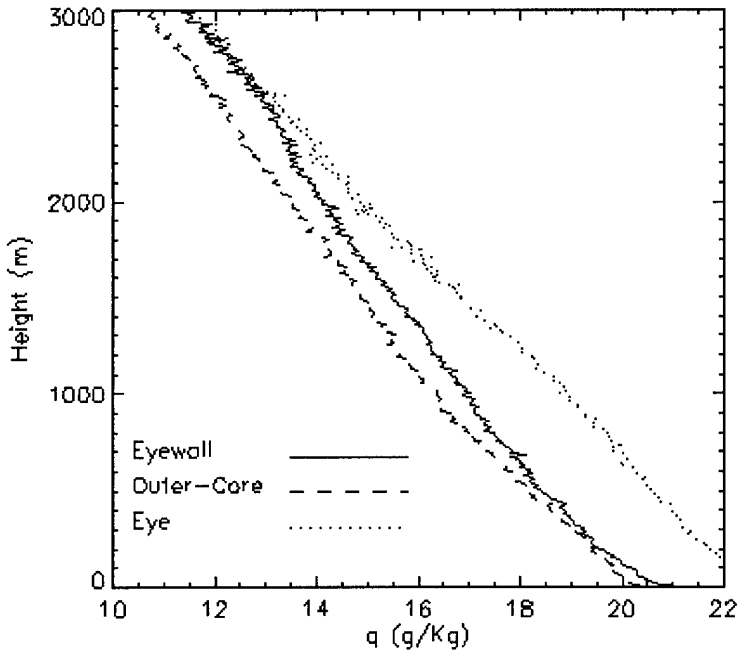

Figure 5.4: Specific humidity profiles with 10-meter averaging from all 6 hurricanes. Solid line-eyewall (92 sondes), dashed-outer core (163 sondes), and dotted-eye (36 sondes).

5.3 Equivalent Potential Temperature Profiles

The main purpose of looking at equivalent potential temperature is to evaluate the degree of buoyancy within tropical cyclones. Figure 5.5 shows from these 6 storms what others (Gray 2000) have observed with the use of aircraft data; that the θ_e profiles within the eyewall lies between 355-360K (Figure 5.6). These values suggest that the historically assumed 1°C temperature difference between the sea surface and the surface air temperature is not accurate. If air parcels were 1°C colder than the sea surface temperature and the relative humidity was 93%, θ_e values would be about 378°K. However, as shown by Gray (2000) in figure 5.6 and as seen in figure 5.5, θ_e values lie in the 355-360K range in the eyewall. This suggests that the air temperature underneath the eyewall cloud would have to be 3-4° C cooler than the sea in order to obtain the θ_e profiles that are observed. Although airborne expendable bathothermal graphs (AXBTs) were launched into these storms the data is not available at this time to do a direct comparison. However, in the next section it will be shown that the air-sea temperature difference does lie in the 3-4° C range on a climatology basis for these storms.

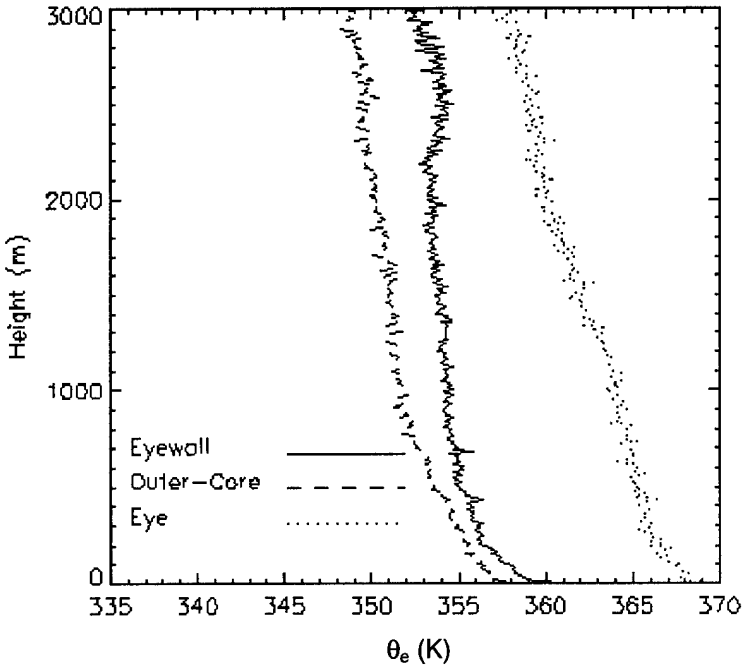

Figure 5.5: Equivalent potential temperature profiles with 10-meter averaging from all 6 hurricanes. Solid line-eyewall (92 sondes), dashed-outer core (163 sondes), and dotted-eye (36 sondes).

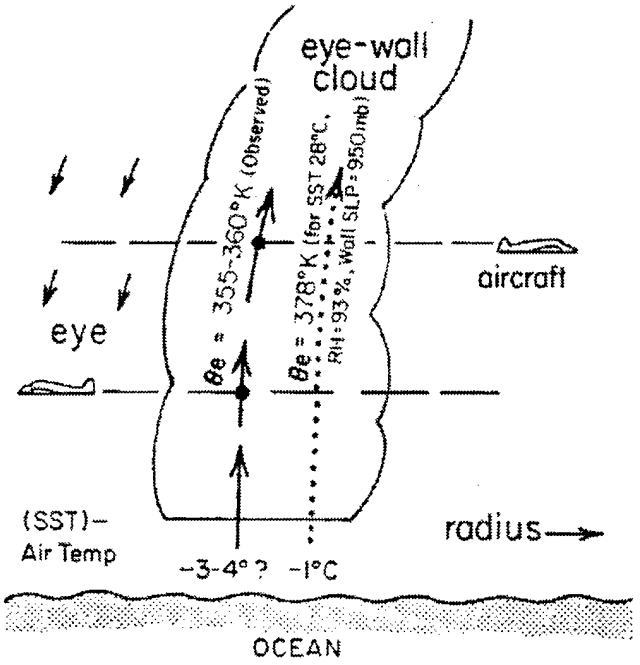

Figure 5.6: Illustration of aircraft observed average eyewall cloud θ_e values (~ 355-360°K) and θ_e values for undiluted parcel ascent assuming the boundary layer is 1°C colder than the ocean sea surface temperature with a surface relative humidity is of 93 percent (378°K). From Gray (2000).

5.4 Eyewall Surface Thermodynamic Parameters

Table 5.1 shows the surface atmospheric parameters of temperature, specific humidity, θ_e, and potential temperature for these storms in the eyewall region. The 92-sonde data set was reduced to 88 in order to only work with observations that reached within 10 meters of the surface. To measure the degree of fit to these values for the small data population, histograms were created for each of these thermodynamic parameters (Figures 5.7-5.10). From the probability distribution functions for these parameters it is seen that 50% of the values for temperature lie between 24.25 and 25.75°C, for potential temperature over 75% of the values lie in the range of 298.5 to 301.5K, for specific humidity nearly 70% of the values lie between 19.75 and 21.75g/Kg, and for θ_e over 75% values lie in the range of 352.5 and 362.5K. These values provide credence to the mean values provided in table 5.1.

Table 5.1: Surface thermodynamic parameters for (88) eyewall dropsondes from all 6 hurricanes from the 1997 and 1998 seasons. Surface values are at 10 meters or less in height.

Storm	Temperature (C)	Specific Humidity (g/Kg)	èe (K)	è (K)
BONNIE	25.7	20.6	359.0	300.4
DANIELLE	25.3	20.4	356.9	299.2
ERIKA	25.3	20.9	360.3	300.8
GEORGES	25.2	21.5	363.5	301.9
GUILLERMO	25.8	21.1	363.1	302.5
MITCH	24.3	20.4	359.1	301.0
Mean	25.3	20.7	359.5	300.6
Max	27.0	23.8	371.0	303.8
Min	23.5	18.1	350.1	297.3

Figure 5.11 shows that the rule of thumb that the air to sea temperature difference is not 1°C as suggest by Gray (2000). Table 5.2 shows the calculated air temperatures, the sea surface temperature derived from a climatological atlas that covered over 80 years of data from 1900-1979 (Sadler et al. 1987), and the air-sea temperature difference. Overall, the storms the mean air-sea temperature difference was -3.2°C, which agrees with of Gray (2000) and figure 5.11.

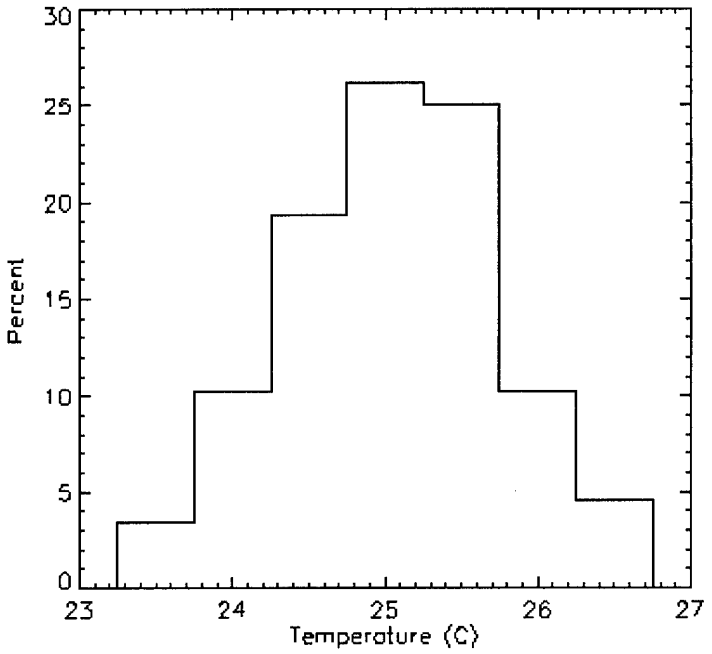

Figure 5.7: Histogram of eyewall temperature for 88 sondes that reached within 10 meters of the sea surface from storms from the 1997 and 1998 seasons. Bin size of 0.5°C.

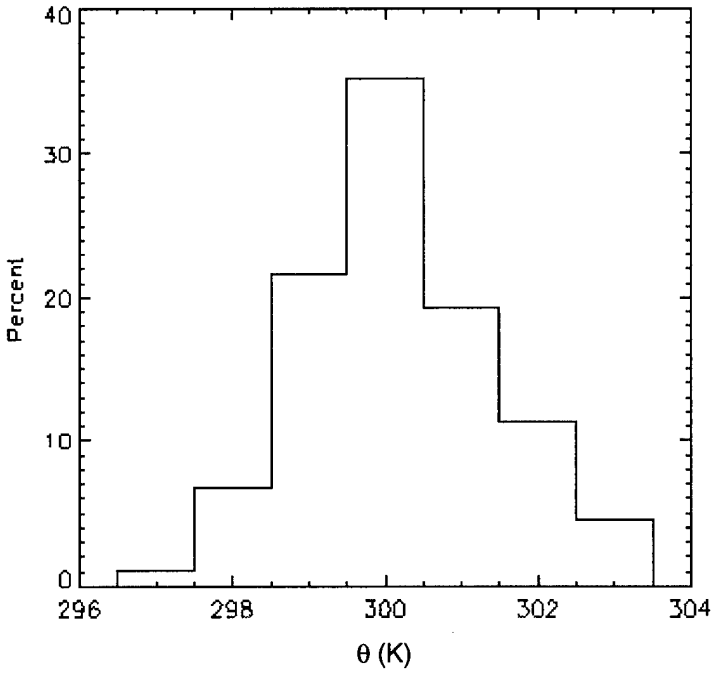

Figure 5.8: Histogram of eyewall potential temperature for 88 sondes that reached within 10 meters of the sea surface from storms from the 1997 and 1998 seasons. Bin size 1.0°C.

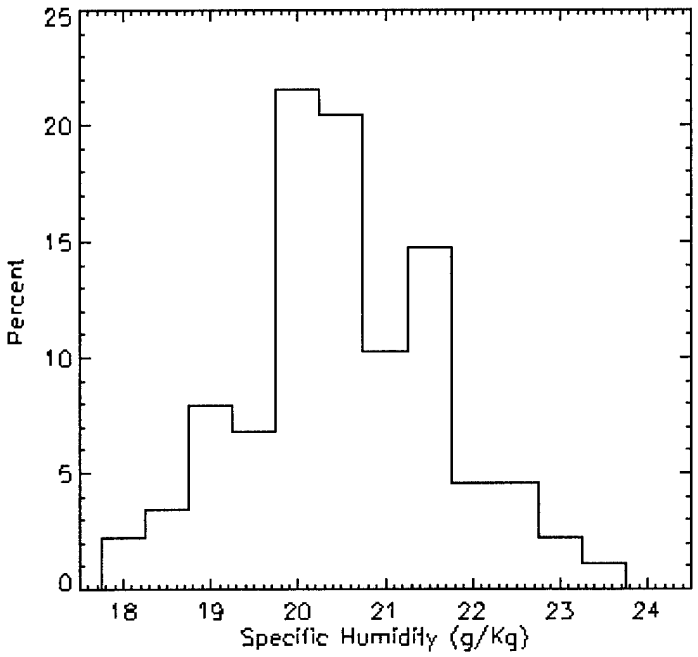

Figure 5.9: Histogram of eyewall specific humidity for 88 sondes that reached within 10 meters of the sea surface from storms from the 1997 and 1998 seasons. Bin size of 0.5°C.

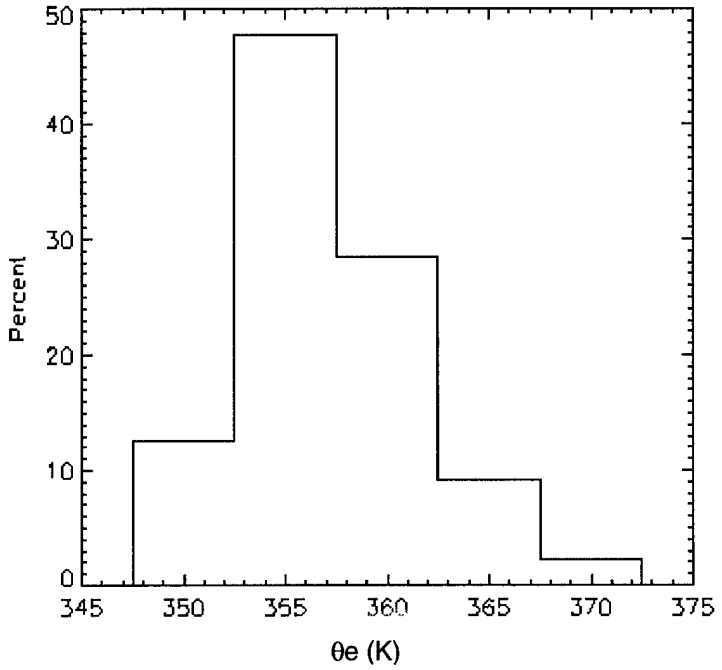

Figure 5.10: Histogram of eyewall θ_e for 88 sondes that reached within 10 meters of the sea surface from storms from the 1997 and 1998 seasons. Bin size of 5.0°C.

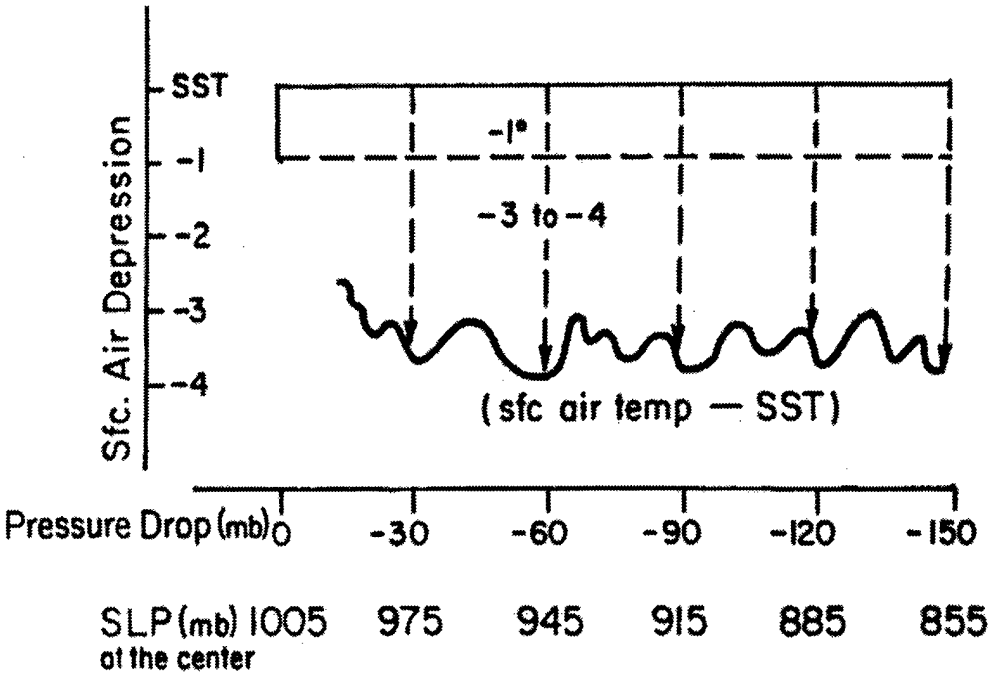

Figure 5.11: Estimated sea minus air temperature difference (°C) under the wall cloud (Gray 2000).

Table 5.2: Average temperatures per storm, corresponding sea-surface temperatures, and air-sea temperature differences.

Storm	Air Tempearature (C)	Sea Temperature (C)	Air - Sea Difference (C)
BONNIE	25.7	28.4	-2.7
DANIELLE	25.3	28.6	-3.3
ERIKA	25.3	28.3	-3.0
GEORGES	25.2	28.1	-2.9
GUILLERMO	25.8	29.0	-3.2
MITCH	24.3	28.5	-4.2
Mean	25.3	28.5	-3.2

Additionally, derived θ_e calculations were performed. By taking the average eyewall pressure, the climatology sea surface temperature, and assuming saturated conditions at the surface, θ_e was calculated on a per storm basis (Table 5.3). The results confirm what Gray (2000) sug-

gested from figure 5.6, that with air-sea temperature difference of ~ -3°C theta-e values would lie in the 355-360K range, significantly less than if the air-sea temperature difference was only 1°C.

Table 5.3: θ_e values from the dropwindsonde data, calculated from climatology, and calculated air-sea θ_e differences.

Storm	Air θ_e (K)	Sea θ_e (K)	Air-Sea θ_e (K) Difference
BONNIE	359.0	376.9	-17.9
DANIELLE	356.9	376.3	-19.4
ERIKA	360.3	378.4	-18.1
GEORGES	363.5	379.9	-16.4
GUILLERMO	363.1	385.3	-22.2
MITCH	359.1	382.8	-23.7
Mean	359.5	379.9	-19.6

5.5 Summary and Discussion

It was shown that the air-sea temperature differences lie in the range of 3-4°C as suggested by Gray (2000) and Anthes (1982). This result alters the concept that surface air temperatures adjust to ocean temperature to within 1°C. Gray (2000) and others have hypothesized that the main mechanism for this temperature difference is due to expansion cooling resulting from air transversing from the outer regions into the eyewall. For a 30mb pressure drop the air would cool approximately 3°C. Sea-spray evaporation could also play some role and this topic is being currently debated. The end result seems to be that the bulk formula (Gray 2000) for sensible heat flux from the ocean to the air cannot keep up with the rate of expansion cooling as air parcels travel into the eyewall region. These findings make it more difficult to explain the buoyancy within the eyewall region.

Chapter 6

CONCLUSIONS

6.1 Summary and Discussion

This study provided a unique look at the radial and tangential winds provided from the GPS dropwindsonde data and storm center fix data. It was found that the observed radial inflow is approximately twice that determined from friction alone. It was also found that the vertical gradient of the radial wind correlates to storm intensity. It is suggested that changes in the vertical gradient of the radial wind would precursor changes in storm intensity. The thermodynamic data show that the actual air-sea temperature difference lies in the range of –3 to -4°C and averaged –3.2°C over the 6 hurricanes from the 1997 and 1998 seasons. This temperature difference confirms the hypothesis of Gray (2000) and others that theta-e profiles in the eyewall region are significantly lower than a 1°C air-sea temperature difference would suggest. The mostly like reason for this difference between the air and sea temperature is from expansion cooling as air transverses down the pressure gradient from the outer-core into the eyewall region. This temperature difference implies that eyewall buoyancy is less than previous believed.

6.2 Future Work

This work contained only a small fraction of the future potential of the number of dropwindsondes that will be dropped into tropical storms and hurricanes. For instance, there were only 94 eyewall dropwindsondes from the 1997 and 1998 seasons, but from the 1999 season alone there were over 263 eyewall dropwindsondes launched (Franklin et al. 2000). This represents almost a 400% increase in eyewall sondes for analysis. With the additional sondes a reanalysis of the radial wind observed to friction should be undertaken to verify these results. Additionally, as the number of dropwindsondes increases a detailed thermodynamic analysis to determine the degree

of buoyancy should also be evaluated as well as its effect on the maximum potential intensity of hurricanes.

Additionally, continued analysis of the gradient of the radial wind inflow for more storms should be undertaken to and see if results shown hold. While it was shown that the degree of the gradient of the radial wind in the lowest 1000 meters indicates storm intensity for these storms, the additional data would also help clarify this correlation. Indeed if various missions were carried out on an individual storm over multiple time periods the change of the gradient of the radial wind could be studied to determine if there is any correlation to changes in storm intensity.

With the aircraft flight data that is now currently available for the 1997 and 1998 seasons a study as done by Weatherford and Gray (1988a,b) where they compared storm strength as defined as the magnitude of the wind in an annulus from 100-300 km from the eye to tropical storm intensity as measured by the maximum sustained wind speed in the eyewall. Weatherford and Gray found that the strengths of tropical storms relate weakly with intensity. However they worked with 0.5-degree resolution data from 1 to 2.5 degrees. The GPS dropwindsondes offer the advantage of choosing any level to determine strength and offer superb aerial coverage.

Many meteorological items of interest can be undertaken for research and in the coming years these data sets are only going to get larger and with it--expanding possibilities.

REFERENCES

Aberson, S. D., and J. L. Franklin, 1999: Impact on hurricane track and intensity forecasts of GPS dropwindsonde observations from the first-season flight of the NOAA gulfstream-IV jet aircraft. *Bull. Amer. Meteor. Soc.*, **80**, 421-427.

Anthes, R. A., 1982: Tropical cyclones, their evolution, structure, and effects. Meteor. Monographs, Vol. **19**, AMS, 45 Beacon Street, Boston, MA, 02108, 208 pp.

Beukers, J. M., 1967: Windfinding using the loran-c and omega long range navigation signals. Supplement, IEEE Transactions on Aerospace and Electronic Systems.

Black M. L. and J. L. Franklin, 2000: GPS dropwindsonde observations of the wind structure in convective and non-convective regions of the hurricane eyewall. *24th Conf. on Hurricanes & Tropical Met.*, Fort Lauderdale, FL, Amer. Meteor. Soc., 448-449.

Burpee, R. W., D. G. Marks and R. T. Merrill, 1984: An assessment of omega dropwindsonde data in track forecasts of hurricane Debby (1982). *Bull. Amer. Meteor. Soc.*, **65**, 1050-1058.

Burpee, R. W. J. L. Franklin, S J. Lord, R. E. Tuleya, and S. D. Aberson, 1996: The impact of omega dropwindsondes on operational hurricane track forecast models. *Bull. Amer. Meteor. Soc*, **77**, 925-933.

Dvorak, V. F., 1975: Tropical cyclone intensity analysis and forecasting from satellite imagery. *Mon. Wea. Rev.*, **103**, 420-430.

Dvorak, V. F., 1984: Tropical cyclone intensity analysis using satellite data. NOAA Technical Report NESDIS 11, U.S. Department of Commerce, National Oceanic and Atmospheric Administration, National Environmental Satellite, data, and Information Service, Washington, D. C., 20233, 47 pp.

Eastin, M. D. 1999: Instrument wetting errors in hurricanes and a re-examination of inner-core thermodynamics. Colorado State Department of Atmospheric Science ,Report **683**.

Franklin, J. L. 1990: Dropwindsonde observation of the environmental flow of Hurricane Josephine (1984) relationships to vortex motion. *Mon. Wea. Rev.*, **118**, 2732-2744.

Franklin, J. L. and M. DeMaria, 1992: The impact of omega dropwindsonde observations on barotropic hurricane track forecasts. *Mon. Wea. Rev.*, **120**, 381-391.

Franklin, J. L., H. L. Cole, D. K. Lauritsen, K. D. Norris, E. F. Chamberlain, 1997: GPS dropwindsondes and the NOAA G-IV jet aircraft: New opportunities for forecasting and research. *22nd Conf. on Hurricanes & Tropical Met.*, Fort Collins, CO, Amer. Meteor. Soc., 135-136.

Franklin, J. L., M. L. Black, and S. E. Feuer, 1999: Wind profiles in hurricanes determined by GPS dropwindsondes. *23rd Conf. on Hurricanes & Tropical Met.*, Dallas, TX, Amer. Meteor. Soc., 167-168.

Franklin, J. L., M. L. Black, and K. Valde, 2000: Eyewall wind profiles in hurricanes determined by GPS dropwindsondes. *2000 National Hurricane Conference*, New Orleans, LA, 17-21 April 2000, 24-25.

Franklin, J. L., M. L. Black, and K. Valde, 2000: Eyewall wind profiles in hurricanes determined by GPS dropwindsondes: *24th Conf. on Hurricanes & Tropical Met.*, Fort Lauderdale, FL, Amer. Meteor. Soc., 446-447.

George, J. E., and W. M. Gray, 1976: Tropical cyclone motion and surrounding parameter relationships. *J. Appl. Meteor.*, **15**, 1252-1264.

Gray, W. M., 2000: Tropical Cyclones, World Meteorological Organization, in preparation.

Heming, J. T. 1999: The impact of dropsondes on UK meteorological office global model forecasts of hurricanes Erika and Linda. *23rd Conf. on Hurricanes & Tropical Met.*, Dallas, TX, Amer. Meteor. Soc., 830-833.

Hock, T. F., H. L. Cole, and K. D. Norris, 1995: The new NCAR GPS dropwindsonde. *9th Symposium. On Meteorological Observations and Instrumentation*, Charlotte, NC, Amer. Meteor. Soc., 70-74.

Hock, T. F., D. Lauritsen, K. Norris, E. Chamberlain, 1998: Airborne vertical atmospheric profiling system (AVAPS). *10th Symposium. On Meteorological Observations and Instrumentation*, Phoenix, AZ, Amer. Meteor. Soc., 32-37.

Hock, T. F., and J. L. Franklin, 1999: The NCAR GPS dropwindsonde. *Bull. Amer. Meteor. Soc.*, **80**, 407-420.

Kaisti, K. 1995: New low cost GPS-Solution for upper air wind finding. *9th Symposium. On Meteorological Observations and Instrumentation*, Charlotte, NC, Amer. Meteor. Soc., 16-20.

Lally, V. E., D. K. Lauritsen, T. F. Hock, and K. D. Norris, 1989: Wind measurements over the North Atlantic using a loran-c dropwindsonde. *Navigation: Journal of The Institute of Navigation*, **36**, 363-372.

LeeJoice, R. L., 2000: Hurricane radial wind profiles derived from GPS dropwindsonde data. *24th Conf. on Hurricanes & Tropical Met.*, Fort Lauderdale, FL, Amer. Meteor. Soc., 452-453.

Powell, M. D., P. G. Black, and S.H. Houston, 1999: GPS sonde insights on boundary layer structure in hurricanes. *23rd Conf. on Hurricanes & Tropical Met.*, Dallas, TX, Amer. Meteor. Soc., 881-884

Saarnimo, T.: 1998: GPS The global windfinding method. *10th Symposium. On Meteorological Observations and Instrumentation*, Phoenix, AZ, Amer. Meteor. Soc., 51-54.

Saffir, H. and R. Simpson, 1974: The hurricane disaster potential scale. *Weatherwise*, August 1974, 169-170.

Sadler, J. C., M. A. Lander, A. M. Hori, and L. K. Oda, 1987: Tropical marine climatic atlas-Indian ocean and Atlantic ocean. Dept. of Met., University of Hawaii, UHMET, **1**, 87-01.

Simpson, R. H., P. K. Govind, and R. Holle, 1975: The GATE dropwindsonde program. Bull. Amer. Soc., 56, 984-987.

Tuleya, R. E., and S. J. Lord, 1997: The impact of dropwindsonde data on GFDL hurricane model forecasts using global analyses. *Wea. Forecasting.*, **12**, 307-323.

White, S. R., J. D. Mc Fadden, and J. L. Franklin, 1998: Atmospheric observations with the NOAA gulfstream IV-SP. *10th Symp. on Met. Observ. & Instr.*, Somewhere, US, 38-41.

Weatherford, C. and W. M. Gray, 1998: Typhoon structure as revealed by aircraft reconnaissance. Part I: Data analysis and climatology. *Mon. Wea. Rev.*, **116**, 1032-1043.

Weatherford, C. and W. M. Gray, 1988: Typhoon structure as revealed by aircraft reconnaissance. Part II: Structural variability. *Mon. Wea. Rev.*, **116** 1044-1056.

Willoughby, H. E., and M. B. Chelmow, 1982: Objective determination of hurricane tracks from aircraft observations. *Mon. Wea. Rev.*, **110**, 1298-1305.

Appendix A

Dropwindsonde Data Files

A.1 Data Amount

HRD is responsible for processing, cataloging and maintaining all dropwindsonde data. For the years 1997 and 1998 alone, over 1,150 dropwindsondes were launched into 10 named storms. Of the named storms that reached hurricane status, over 972 dropwindsondes were launched (Table 3.1). The amount of data that each dropwindsonde takes depends on the sampling rate and the pressure at which the sonde is launched. The sampling rate is twice a second and the launch pressure varies by the type of aircraft and then on the mission parameters. Table A.1 shows that the number of observations taken increases rapidly with decreasing launch pressure. This is especially the case for the G-IV missions that provide the 'synoptic flow' measurements flying at flight levels around 200 mb.

Table A.1: Approximate number of observations taken per dropwindsonde corresponding to the height (pressure) of the launch.

Observations	Pressure
1500	200
1000	450
600	600
300	750

A.2 Data File Types

All data is stored by storm name and then by the mission number flown into the storm. For each mission there are three main types of data files: mission summaries, catalog files, and individual dropwindsonde data files. The mission summaries provide a brief synopsis of the mission times, aircraft involved, take-off times, scientific crew, the type of experiment; Synoptic Flow, Vortex

Motion and Evolution, etc., and a brief listing of any significant hardware problems. Each mission has a corresponding catalog file that contains the sequence of the dropsondes launched during the mission. Table A.2 is an example of a catalog file for the mission 19981027I. The mission id is composed of the year, month, date, and aircraft that performed the mission. H and I suffixes refer to the two P-3s and the suffix N is for the G-IV aircraft missions. Additionally, the catalog file also contains the serial number of the sondes used, the launch latitude, longitude, and pressure level, as well as any comments concerning the sonde as entered by the mission specialists. The comment section provides great insight on where the dropwindsondes were launched. The mission specialists usually remark the eyewall soundings (as seen from sequence 9 in table A.2); this makes finding eyewall drops immeasurably easier because no corresponding satellite imagery processing is needed to determine dropsonde eyewall launches.

The individual dropwindsondes data files contain the actual atmospheric measurements. Table A.3 illustrates the format of a dropwindsonde file from the sonde (highlighted in table A.2) that fell through the east eyewall of hurricane Mitch. Each file contains a header section that contains information on type of calibrations used, any comments, and some repeated information contained in the catalog file. The atmospheric measurements section follows with information consisting of an index, time since launch, pressure, temperature, relative humidity, geopotential height, wind speed, wind direction, u and v components of the wind, latitude, and longitude. Lastly, flags for errors in temperature, pressure, relative humidity, and wind measurements are contained in this section.

Table A.2: Catalog file of GPS dropwindsondes dropped on October 27st, 1998 into Hurricane Mitch.

CATALOG OF PROCESSED DROPWINDSONDES FOR 19981027I

Seq	Serial #	Date/Time (UTC)	Lat (N)	Lon (W)	Pr (mb)	Comments
1	983310025	981027/202333	21.98	85.5	504	Poor GPS.
2	983410124	981027/212857	16.92	85.78	679	NW eyewall.
3	983310027	981027/213312	16.69	85.59	655	Eye.
4	981040049	981027/213636	16.52	85.41	668	SE wall. Poor GPS.
5	983310121	981027/213911	16.41	85.29	686	SE eyewall. Super near surface.
6	983340064	981027/215318	16.68	84.79	695	50 nm E of center.
7	983340066	981027/220330	16.71	85.26	681	E wall.
8	983340078	981027/220355	16.71	85.28	676	E wall.
9	974530045	981027/220423	16.7	85.32	673	E wall.
10	981040046	981027/221223	16.67	85.89	689	Winds very intermittent, hence long filter.
11	982720392	981027/222105	16.59	86.43	697	Mixed RH, poor GPS.
12	983410111	981027/223448	16.48	85.9	683	SW wall.
13	983340050	981027/224250	16.76	85.45	666	NE wall.
14	974910010	981027/224311	16.78	85.43	668	Assumed to not reach sfc. NE wall. Split RH.
15	983410045	981027/224330	16.8	85.41	672	NE wall.
16	973840047	981027/230601	16.91	85.6	676	N wall.
17	983410106	981027/230633	16.88	85.61	675	N wall.
18	983310142	981027/230731	16.82	85.61	677	N wall. Split RH sensor.
19	983310127	981027/231352	16.37	85.6	668	S wall.
20	981810013	981027/232125	15.99	85.44	695	50 nm south.
21	983340068	981027/233547	16.47	85.32	675	SE wall.
22	983340088	981027/233635	16.48	85.37	672	SE wall. Big updrafts. Poor GPS.
23	983340063	981027/233712	16.5	85.4	671	SE wall. Poor GPS.
24	982720319	981027/233954	16.57	85.58	659	Eye.
25	972630028	981027/234436	16.72	85.86	696	NW wall.
26	983410126	981028/001452	16.47	85.68	505	Inside eye.
27	983340065	981028/001608	16.52	85.6	504	Near center of eye.
28	983310180	981028/001709	16.58	85.53	504	Inside eye.
29	982720393	981028/001800	16.64	85.52	504	Inside eye, but intersects wall.
30	983410113	981028/002903	16.73	85.57	503	Inner edge/eye, intersects eyewall.
31	981040005	981028/003143	16.93	85.57	510	Outer eyewall/rainband.

Table A.3: Sample Dropwindsonde Data File for sonde 974530045 within Hurricane Mitch, Oct 27st, 1998.

DROPWINDSONDE PROCESSING RECORD Sonde: 974530045
PDS file written Oct 29, 1998. Format: V3.14
Aircraft: N43RF Date: 981027 Time: 220423 UTC

Bias corrections: PR = .0 mb TE = .0 C RH = .0 % PRB = .0 mb
Filters (LPF): PTH = 5 s WIND = 5 s Hyd anchor = SFC
RH T-compensation = Y WSHR COR = Y Splash PR = 956.6 mb
Estimated PR used = N GPS VERR = .77 m/s HYD SFCP = 962.0 mb
Dyn T correction = Y WGACORR = -1.8 m AC GA ADJ = .0 m

COMMENTS: E wall.

Date: 981027 Lat: 16.70 N TA: 9.7 C PS: 673.8 mb WD: 170 deg
Time: 220423 Lon: 85.32 W TD: -999.0 C GA: 3050 m WS: 64.7 m/s
SID: 974530045 RH: -999.0 % Navaid: GP

IX	t (s)	P (mb)	T (C)	RH (%)	Z (m)	WD	WS (m/s)	U (m/s)	V (m/s)	NS	WZ (m/s)	ZW (m)	FP	FT	FH	FW	LAT (N)	LON (E)
1	0.1	674.3	9.75	-999	3001	170	64.65	-11.26	63.67	-999	-999	2999	3	3	0	3	16.704	-85.315
2	0.6	674.8	9.83	-999	2994	170	64.49	-11.36	63.48	-999	-999	2993	3	3	0	3	16.704	-85.315
3	1.1	675.3	9.89	-999	2988	170	64.44	-11.39	63.43	-999	-999	2986	3	3	0	3	16.704	-85.315
4	1.6	675.9	9.96	-999	2982	170	64.4	-11.42	63.38	-999	-999	2980	3	3	0	3	16.704	-85.315
5	2.1	676.4	10.02	-999	2975	170	64.35	-11.44	63.33	-999	-999	2974	3	3	0	3	16.705	-85.315
6	2.6	676.9	10.08	-999	2969	170	64.3	-11.47	63.27	-999	-999	2967	3	3	0	3	16.705	-85.315
7	3.1	677.4	10.15	-999	2963	170	64.26	-11.5	63.22	-999	-999	2961	3	3	0	3	16.705	-85.315
8	3.6	677.9	10.21	-999	2956	170	64.21	-11.52	63.17	-999	-999	2955	3	3	0	3	16.706	-85.315
9	4.1	678.4	10.28	-999	2950	170	64.17	-11.55	63.12	-999	-999	2948	3	3	0	3	16.706	-85.315
10	4.6	678.9	10.34	-999	2944	170	64.12	-11.58	63.07	-999	-999	2942	3	3	0	3	16.706	-85.316
11	5.1	679.5	10.41	-999	2938	170	64.08	-11.61	63.02	-999	-999	2936	3	3	0	3	16.706	-85.316
12	5.6	680	10.47	-999	2931	170	64.03	-11.63	62.96	-999	-999	2929	3	3	0	3	16.707	-85.316
13	6.1	680.5	10.53	-999	2925	169	63.98	-11.66	62.91	-999	-999	2923	3	3	0	3	16.707	-85.316
14	6.6	681	10.6	-999	2919	169	63.94	-11.69	62.86	-999	-999	2917	3	3	0	3	16.707	-85.316
15	7.1	681.5	10.66	-999	2912	169	63.89	-11.72	62.81	-999	-999	2910	3	3	0	3	16.708	-85.316
16	7.6	682	10.72	-999	2906	169	63.85	-11.74	62.76	-999	-999	2904	3	3	0	3	16.708	-85.316
*	*	*	*	*	*	*	*	*	*	*	*	*	*	*	*	*	*	*

Table A.3 continued: Sample Dropwindsonde Data File for sonde 974530045 within Hurricane Mitch, Oct 27th, 1998.

449	224.1	934.1	21.77	100	215	97	74.35	-73.74	9.44	5	2.5	213	0	0	0	0	16.805	-85.396
450	224.6	934.6	21.8	100	210	98	74.21	-73.55	9.89	5	2.5	208	0	0	0	0	16.805	-85.396
451	225.1	935.2	21.84	100	205	98	73.9	-73.15	10.49	4	2.4	203	0	0	0	0	16.805	-85.396
452	225.6	935.7	21.87	100	199	99	73.31	-72.47	11.1	5	2.3	198	0	0	0	0	16.805	-85.397
453	226.1	936.3	21.91	100	194	99	72.37	-71.44	11.58	5	2.1	192	0	0	0	0	16.805	-85.397
454	226.6	936.9	21.95	100	189	100	71.09	-70.09	11.85	6	2	187	0	0	0	0	16.805	-85.397
455	227.1	937.4	21.99	100	183	100	69.57	-68.55	11.88	6	1.9	182	0	0	0	3	16.805	-85.398
456	227.6	938	22.04	100	178	100	68.06	-67.04	11.75	5	1.8	176	0	0	0	0	16.805	-85.398
457	228.1	938.6	22.09	100	172	100	66.85	-65.84	11.54	5	1.7	171	0	0	0	0	16.805	-85.398
458	228.6	939.2	22.14	100	167	100	66.23	-65.25	11.35	5	1.6	165	0	0	0	0	16.805	-85.399
459	229.1	939.8	22.19	100	161	100	66.41	-65.45	11.23	5	1.6	159	0	0	0	0	16.805	-85.399
460	229.6	940.4	22.24	100	156	100	67.39	-66.44	11.23	5	1.5	154	0	0	0	0	16.806	-85.399
461	230.1	941	22.3	100	150	99	68.95	-68.01	11.34	4	1.4	148	0	0	0	0	16.806	-85.4
462	230.6	941.6	22.36	100	145	99	70.72	-69.77	11.52	5	1.2	143	0	0	0	3	16.806	-85.4
463	231.1	942.2	22.43	100	139	99	72.22	-71.27	11.68	6	1	137	0	0	0	0	16.806	-85.4
464	231.6	942.8	22.5	100	133	99	73.02	-72.08	11.67	6	0.8	131	0	0	0	0	16.806	-85.401
465	232.1	943.5	22.59	100	127	99	72.84	-71.94	11.37	6	0.5	125	0	0	0	0	16.806	-85.401
466	232.6	944.2	22.68	100	121	99	71.59	-70.79	10.7	6	0.2	119	0	0	0	0	16.806	-85.401
467	233.1	944.8	22.77	100	115	98	69.5	-68.82	9.69	5	0	113	0	0	0	0	16.806	-85.402
468	233.6	945.5	22.86	100	108	97	66.97	-66.43	8.5	5	-0.2	106	0	0	0	0	16.806	-85.402
469	234.1	946.3	22.94	100	102	97	64.52	-64.1	7.36	5	-0.3	100	0	0	0	0	16.806	-85.402
470	234.6	947	23.01	100	95	96	62.59	-62.25	6.47	6	-0.3	93	0	0	0	3	16.806	-85.403
471	235.1	947.7	23.08	100	88	95	61.36	-61.08	5.84	6	-0.2	87	0	0	0	0	16.806	-85.403
472	235.6	948.4	23.14	100	82	95	60.8	-60.57	5.31	6	0	80	0	0	0	0	16.806	-85.403
473	236.1	949.1	23.19	100	76	94	60.63	-60.45	4.67	6	0.2	74	0	0	0	0	16.806	-85.403
474	236.6	949.7	23.23	100	69	94	60.68	-60.56	3.79	7	0.6	68	0	0	0	0	16.806	-85.404
475	237.1	950.4	23.26	100	63	93	61	-60.94	2.75	7	1.1	61	0	0	0	0	16.806	-85.404
476	237.6	951	23.29	100	58	91	61.68	-61.67	1.56	7	1.6	56	0	0	0	0	16.806	-85.404
477	238.1	951.6	23.32	100	52	90	62.65	-62.65	0.2	7	2.2	50	0	0	0	0	16.806	-85.405
478	238.6	952.2	23.36	100	47	89	63.88	-63.88	-0.83	6	2.9	45	0	0	0	0	16.806	-85.405
479	239.1	952.7	23.4	100	42	89	63.78	-63.76	-1.38	6	3.5	40	0	0	0	0	16.806	-85.405
480	239.6	953.2	23.46	100	38	-999	-999	-999.00	- 999	-999	4	36	0	0	0	0	16.806	-85.405
481	240.1	953.6	23.52	100	34	-999	-999	-999.00	- 999	-999	4.2	32	0	0	0	0	16.806	-85.406
482	240.6	954	23.59	100	30	-999	-999	-999.00	- 999	-999	4.3	29	0	0	0	0	16.806	-85.406
483	241.1	954.3	23.66	100	27	-999	-999	-999.00	- 999	-999	3.7	25	0	0	0	0	16.806	-85.406
484	241.6	954.8	23.74	100	23	-999	-999	-999.00	- 999	-999	3.7	21	0	0	0	0	16.806	-85.407
485	242.1	955.3	23.82	100	18	-999	-999	-999.00	- 999	-999	3.5	16	0	0	0	0	16.806	-85.407
486	242.6	955.8	23.94	100	14	-999	-999	-999.00	- 999	-999	3.1	12	3	3	3	0	16.806	-85.407
487	243.1	956.6	24.12	100	7	-999	-999	-999.00	- 999	-999	2.5	5	0	0	0	0	16.806	-85.407